



UNIVERSITY OF LEEDS

This is a repository copy of *Behavior of S, SO, and SO<sub>3</sub> on Pt (001), (011), and (111) surfaces: A DFT study.*

White Rose Research Online URL for this paper:  
<https://eprints.whiterose.ac.uk/174224/>

Version: Accepted Version

---

**Article:**

Ungerer, MJ, van Sittert, CGCE and de Leeuw, NH [orcid.org/0000-0002-8271-0545](https://orcid.org/0000-0002-8271-0545) (2021) Behavior of S, SO, and SO<sub>3</sub> on Pt (001), (011), and (111) surfaces: A DFT study. The Journal of Chemical Physics, 154 (19). 194701. ISSN 0021-9606

<https://doi.org/10.1063/5.0043501>

---

© 2021 Author(s). This is an author produced version of an article published in The Journal of Chemical Physics . Uploaded in accordance with the publisher's self-archiving policy.

**Reuse**

Items deposited in White Rose Research Online are protected by copyright, with all rights reserved unless indicated otherwise. They may be downloaded and/or printed for private study, or other acts as permitted by national copyright laws. The publisher or other rights holders may allow further reproduction and re-use of the full text version. This is indicated by the licence information on the White Rose Research Online record for the item.

**Takedown**

If you consider content in White Rose Research Online to be in breach of UK law, please notify us by emailing [eprints@whiterose.ac.uk](mailto:eprints@whiterose.ac.uk) including the URL of the record and the reason for the withdrawal request.



[eprints@whiterose.ac.uk](mailto:eprints@whiterose.ac.uk)  
<https://eprints.whiterose.ac.uk/>

1 **Behaviour of S, SO and SO<sub>3</sub> on Pt (001), (011) and (111) surfaces: A DFT Study**2 Marietjie J. Ungerer,<sup>1,2</sup> Cornelia G.C.E. van Sittert <sup>\*1</sup> and Nora H. de Leeuw <sup>\*2,3</sup>3 <sup>1</sup> Laboratory for Applied Molecular Modelling, Research Focus Area: Chemical Resource Beneficiation, North-  
4 West University, Private Bag X6001, Potchefstroom, 2520, South Africa5 <sup>2</sup> School of Chemistry, Cardiff University, Main Building, Park Place, Cardiff CF10 3AT, United Kingdom6 <sup>3</sup> School of Chemistry, Faculty of Engineering and Physical Sciences, University of Leeds, Leeds LS2 9JT, United  
7 Kingdom8 \*(CGCEvS) E-mail address: [cornie.vansittert@nwu.ac.za](mailto:cornie.vansittert@nwu.ac.za)9 \*(NHdL) E-mail address: [n.h.deleeuw@leeds.ac.uk](mailto:n.h.deleeuw@leeds.ac.uk)

10

11 **Abstract**12 In the hybrid sulphur (HyS) cycle, the reaction between SO<sub>2</sub> and H<sub>2</sub>O is manipulated to produce hydrogen,  
13 with water and sulphuric acid as by-products. However, sulphur poisoning of the catalyst has been widely  
14 reported to occur in this cycle, which is due to strong chemisorption of sulphur on the metal surface. The  
15 catalysts may deactivate as a result of these impurities present in the reactants or incorporated in the  
16 catalyst during its preparation and operation of the HyS cycle.17 Here, we report a density functional theory (DFT) investigation of the interaction between S, SO and SO<sub>3</sub>  
18 with the Pt (001), (011) and (111) surfaces. First, we have investigated the adsorption of single gas phase  
19 molecules on the three Pt surfaces. During adsorption, the 4F hollow sites on the (001) and (011) surfaces  
20 and the fcc hollow site on the (111) surface were preferred. S adsorption followed the trend of (001)<sub>4F</sub> >  
21 (011)<sub>4F</sub> > (111)<sub>fcc</sub>, while SO adsorption showed (001)<sub>4F</sub> > (011)<sub>bridge/4F</sub> > (111)<sub>fcc</sub> and SO<sub>3</sub> adsorption was  
22 most stable in a S,O,O bound configuration on the (001)<sub>4F</sub> > (011)<sub>4F</sub> > (111)<sub>fcc</sub> sites.23 The surface coverage was increased on all the surfaces until a monolayer was obtained. The highest  
24 surface coverage for S shows the trend (001)<sub>S</sub> = (111)<sub>S</sub> > (011)<sub>S</sub>, and for SO it is (001)<sub>SO</sub> > (011)<sub>SO</sub> >  
25 (111)<sub>SO</sub>, similar to SO<sub>3</sub> where we found (001)<sub>SO3</sub> > (011)<sub>SO3</sub> > (111)<sub>SO3</sub>. These trends indicate that the  
26 (001) surface is more susceptible to S species poisoning. It was also evident that both the (001) and  
27 (111) surfaces were reactive towards S, leading to the formation of S<sub>2</sub>. High coverage of SO<sub>3</sub> showed the  
28 formation of SO<sub>2</sub> and SO<sub>4</sub>, especially on the (011) surface. The thermodynamics indicated that an  
29 increased temperature up to 2000 K resulted in Pt surfaces fully covered with elemental S. The SO  
30 coverage showed  $\theta \geq 1.00$  on both the (001) and (011) surfaces, and  $\theta = 0.78$  for the (111) in the  
31 experimental region where the HyS cycle is operated. Lower coverages of SO<sub>3</sub> were observed due to the  
32 size of the molecule.

33

34 **1. Introduction**

35 The oxidation of sulphur dioxide ( $\text{SO}_2$ ) in aqueous solutions has been studied for over a century [1–3].  
36 With the advent of industrialisation, automation and massive population growth, the presence of  $\text{SO}_2$  has  
37 increased not only as a by-product of industry, but also as a result of the uses of new technologies in  
38 everyday life [4,5]. It has been shown that atmospheric  $\text{SO}_2$  has a detrimental effect, not only on the  
39 environment but also human life [5,6]. With more countries and governments enforcing limitations on  
40 industry to reduce  $\text{SO}_2$  emissions [5–7], new technologies are emerging for either the capture [8] or re-  
41 utilisation of  $\text{SO}_2$  [9,10].

42 One viable option for the utilisation of  $\text{SO}_2$  is in the hybrid sulphur (HyS) cycle, where  $\text{SO}_2$  reacts with  
43 water ( $\text{H}_2\text{O}$ ) at temperatures between 80 and 120 °C to form sulphuric acid ( $\text{H}_2\text{SO}_4$ ) and hydrogen ( $\text{H}_2$ ).  
44 The  $\text{H}_2\text{SO}_4$  can be re-utilised by thermal decomposition (> 800 °C) to form oxygen ( $\text{O}_2$ ),  $\text{H}_2\text{O}$  and  $\text{SO}_2$ .  
45 The net reaction of this cycle is therefore the splitting of  $\text{H}_2\text{O}$  into  $\text{O}_2$  and  $\text{H}_2$ . In turn,  $\text{H}_2$  is considered a  
46 potentially viable solution to address sustainable energy production as it is an ideal energy carrier,  
47 especially when coupled with renewable sources and adequate technology [11–14], and it is used in a  
48 variety of applications [15–17].

49 Within the HyS cycle, it is well known that transition metals, even in trace amounts, are needed to catalyse  
50 the  $\text{SO}_2$  oxidation reaction [18–20]. The current catalyst of choice is platinum (Pt), a rare and very  
51 expensive noble metal. While various other metals have been investigated [21], including Cu [22–25], Ni  
52 [26–28], Ag [29,30], Rh [31,32], Pd [24,32–36], in addition to Pt [24,31,37–40], which is still the best  
53 performing catalyst in terms of activity and stability [41–43]. However, major difficulties are still  
54 experienced in experiments, in part due to the occurrence of various co-adsorbed surface sulphur  
55 species, including elemental sulphur (S), sulphur oxide (SO) and sulphur trioxide ( $\text{SO}_3$ ), amongst others  
56 [9].

57 Although sulphur an essential element and the fifth most common element on Earth [3,44], its presence  
58 in a catalytic environment is detrimental, causing lower yields in production and catalyst poisoning [45].  
59 However, very little work has been performed on evaluating the energetics or thermodynamics of the  
60 adsorption of sulphur or sulphur oxides on catalyst surfaces or their surface reactions. In this paper, we  
61 have used density functional theory (DFT) calculations to predict the behaviour of S, SO and  $\text{SO}_3$  on the  
62 Pt (001), (011) and (111) surfaces. We have examined the geometric and electronic properties of the  
63 systems, including the most stable adsorption sites, adsorption modes and possible desorption of species  
64 that may occur, before considering increased surface coverages. Thermodynamic surface phase  
65 diagrams have also been generated by taking into consideration the surface free energies and the  
66 chemical potentials of  $\text{SO}_x$ , ( $x=0,1,3$ ).

## 67 2. Computational Methods

### 68 2.1 Calculation Methods

69 Similar to the method used to study the adsorption of H<sub>2</sub>O and SO<sub>2</sub> [46–48], the Vienna Ab Initio  
70 Simulation Package (VASP) [49–52] version 5.4.1 was used to simulate the Pt surfaces and their  
71 interaction with S, SO and SO<sub>3</sub>. In all calculations, the projector augmented wave (PAW) [53,54]  
72 pseudopotential was used to describe the interaction between the valence and core electrons. The core  
73 electrons were defined up to and including 5p, 3p and 1s orbitals for the Pt, S and O atoms, respectively.  
74 The exchange-correlation approximation was included with the Perdew-Burke-Ernzerhof (PBE) [55]  
75 functional within the generalised gradient approximation (GGA), including the D3-BJ method by Grimme  
76 with Becke-Johnson damping [56] to account for the long-range dispersion interactions [57–61] in these  
77 surface-adsorbate systems. Plane waves were included with the recommended cut-off of 400 eV. The  
78 conjugate gradient technique was adopted for all geometry optimisations and to ensure an electronic  
79 entropy of less than 1 meV.atom<sup>-1</sup>, whereas a smearing of 0.05 eV with the Methfessel-Paxton scheme  
80 order 1 [62] was used to determine the partial occupancies during geometry optimisation. The final static  
81 simulations were obtained with the tetrahedron method with Blöchl corrections [63] to ensure accurate  
82 total energies, charges and densities of states, where the electronic and ionic optimisation criteria were  
83 set at 10<sup>-5</sup> eV and 10<sup>-2</sup> eV.Å<sup>-1</sup>, respectively.

84 The *Fm* $\bar{3}$ *m* crystal structure [64] of Pt was used to construct a bulk Pt structure within a primitive face-  
85 centred cubic (*fcc*) cell. The *k*-point mesh for these calculations was a  $\Gamma$ -centred 17 x 17 x 17 Monkhorst-  
86 Pack mesh [65]. The resulting *fcc* Pt lattice constant was 3.926 Å, which correlates with the experimental  
87 value of 3.925 Å [66,67]. The low Miller index Pt (001), (011) and (111) surfaces were created with the  
88 METADISE code [68]. Periodic p(3 x 3), p(3 x 3) and p(4 x 4) supercells were constructed, respectively,  
89 each with four layers and a 15 Å vacuum space to ensure that no interaction would occur between the  
90 adsorbates and surfaces in neighbouring simulation cells deriving from the 3-dimensional boundary  
91 conditions. All three surfaces are bulk terminated 2x2 structures with four atomic layers, with the surface  
92 simulation cells containing 72, 72 and 64 atoms respectively. The Brillouin zone was sampled by a  $\Gamma$ -  
93 centred 7 x 7 x 1 Monkhorst-Pack *k*-point grid. During the optimisation of the surfaces, the bottom two  
94 layers of the supercells were frozen in their bulk locations, with the remaining two layers allowed to move  
95 until the set energy criteria were met. Even though Pt does not have unpaired electrons, spin polarisation  
96 was considered during these surface calculations, as future work will also include base metals dopants  
97 like Ni and Co, for which this would be necessary.

98 For the calculations of the geometrical properties, adsorption and electronic properties, the isolated S,  
99 SO and SO<sub>3</sub> molecules were modelled in a periodic box of 12 x 13 x 14 Å to ensure negligible interaction  
100 with neighbouring cells. For both the geometry optimisations and energy calculations, the Gaussian

101 smearing [62] of 0.05 eV scheme was used with a  $\Gamma$ -centred Monkhorst-Pack [65]  $k$ -point mesh of 1 x 1  
102 x 1. None of the adsorbate molecules were computed with symmetry constraints, but for increased  
103 accuracy, dipole corrections were added in all directions. Spin polarisation was considered both for the  
104 isolated molecules and in the adsorption calculations. The breakdown of charge transfer between the  
105 adsorbates and the surfaces was obtained via the Bader analysis [69–72], assigning electron density of  
106 molecules and solids to individual atoms or regions enclosed by local minima in the charge density.

## 108 2.2 Coverage-dependent Surface Energies

109 The standard calculation [58,73] of the surface energies for relaxed and unrelaxed systems was used.  
110 To calculate the average adsorption energy ( $E_{ads}$ ) per adsorbate molecule (S, SO and SO<sub>3</sub>) adsorbed  
111 onto the Pt surface, the following equation (1) was used [46–48,74]:

$$112 \quad E_{ads} = \frac{1}{N_{SO_x}} \left[ E_{Pt,r}^{N_{SO_x} \neq 0} - (E_{Pt,r}^{N_{SO_x} = 0} + N_{SO_x} E_{SO_x}) \right], x = 0, 1, 3 \quad (1)$$

113 where  $N_{SO_x}$  is the number of adsorbed S, SO or SO<sub>3</sub> molecules,  $E_{Pt}^{N_{SO_x} \neq 0}$  is the energy of the Pt slab with  
114 adsorbed SO<sub>x</sub> molecules,  $E_{Pt}^{N_{SO_x} = 0}$  is the energy of the clean Pt surface, and  $E_{SO_x}$  is the energy of the  
115 isolated SO<sub>x</sub>, ( $x = 0, 1, 3$ ) molecule after relaxation. Another measure of adsorption is the energy of sequential  
116 adsorption (Sequential  $E_{ads}$ ), [47] indicating the difference in energy as coverage increases:

$$117 \quad Seq. E_{ads} = \left[ E_{Pt,r}^{N_{SO_x} \neq 0(i+1)} - (E_{Pt,r}^{N_{SO_x} \neq 0i} + E_{SO_x}) \right], x = 0, 1, 3, i = 0, 1, \dots N \quad (2)$$

118 thereby calculating the energy difference between that of an adsorbate system with one more adsorbate  
119  $E_{Pt}^{N_{SO_x} \neq 0(i+1)}$  from the previous system with one less adsorbate ( $E_{Pt}^{N_{SO_x} \neq 0(i)}$ ).

120 The surface coverage ( $\theta$ ) is defined as the number of adsorbed SO<sub>x</sub> molecules ( $N_{SO_x}$ ) divided by the  
121 number of adsorption sites (N), as denoted by

$$122 \quad \theta = \frac{N_{SO_x}}{N} \quad (3)$$

123 If no adsorption has taken place,  $\theta = 0$ , whereas for full coverage, i.e. when a monolayer has formed on  
124 the surface,  $\theta = 1$ . The most stable configurations of the (001), (011) and (111) surfaces were used to  
125 investigate surface coverage, with the surface simulation cells having 9, 18 and 9 adsorption sites (N),  
126 respectively. To incorporate the thermodynamics effect of the different coverages of SO<sub>x</sub>, ( $x = 0, 1, 3$ ) on the  
127 Pt (001), (011) and (111) surfaces, the correlating surface free energies ( $\sigma$ ) are compared at different  
128 temperatures (T) and the SO<sub>x</sub>, ( $x = 0, 1, 3$ ) chemical potential ( $\mu_{SO_x}$ ). To this end, we have followed an

129 established method [74] to determine the thermodynamic effect of the adsorption of SO<sub>2</sub> [47,48] and H<sub>2</sub>O  
130 [46] on these Pt surfaces. The resulting change in surface free energy resulting from the SO<sub>x</sub> adsorption  
131 was calculated as follows:

$$132 \quad \Delta\sigma(T, p) = \frac{1}{A_{surface}} [E_{Pt,r}^{N_{SO_x} \neq 0} - E_{Pt,r}^{N_{SO_x} = 0} - N_{SO_x} \cdot \mu_{SO_x}] \quad (4)$$

133 In order to calculate the surface free energy as a function of temperature and pressure, we also require  
134 the chemical potential of the SO<sub>x</sub> species  $\mu_{SO_x}(T, p_0)$ , which we have obtained from experimental values  
135 [46–48], by extracting the chemical potential from ideal gas values in thermodynamic tables [75]. The  
136 chemical potential of SO<sub>x</sub>, ( $x = 0, 1, 3$ ) species in the gas phase has been reported before [76] and can be  
137 expressed as:

$$138 \quad \mu_{SO_x}(T, p) = E_{SO_x}^{ZPE} + \Delta G_{SO_x}(T, p_0) + k_B T \ln \frac{p}{p_0} \quad (5)$$

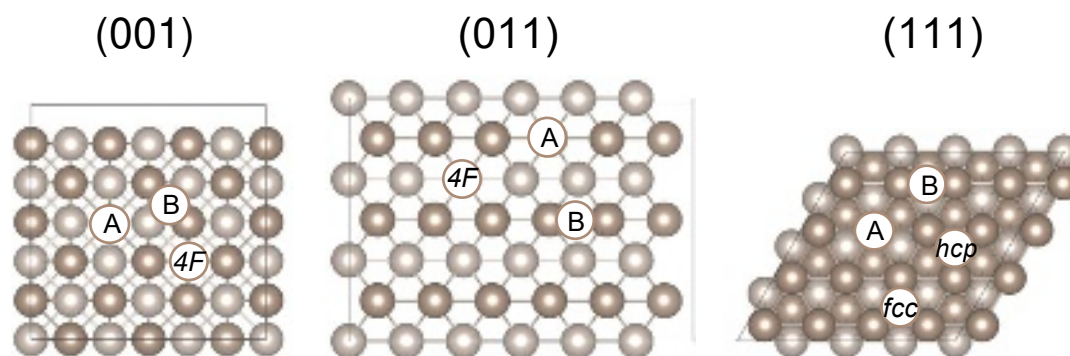
139 Where the zero-point energy  $E_{SO_x}^{ZPE}$  includes the contributions from rotation and vibrations of the SO<sub>x</sub>  
140 molecule, and the Gibbs free energy difference  $\Delta G_{SO_x}(T, p_0)$  is per SO<sub>x</sub> molecule for temperatures  
141 between 0 K and T, at  $p_0 = 1$  bar. The final term ( $k_B T \ln \frac{p}{p_0}$ ) denotes the free energy change of SO<sub>x</sub> gas  
142 at constant temperature (T) when the partial pressure changes from  $p_0$  to  $p$ .

143

### 144 3. Results and Discussion

#### 145 3.1 Pt (001), (011) and (111) surfaces

146 Figure 1 shows the three Pt surfaces under consideration with possible adsorption sites for each surface.  
147 The *fcc* arrangement of Pt resulted in the flat smooth Pt (001) and Pt (111) structures and a corrugated  
148 or grooved Pt (011) surface. The surface energy of each surface correlates with experimental [77] and  
149 modelled values [78] and followed the observed trend Pt (111) < Pt (001) < Pt (011) at 2.046 J/m<sup>2</sup>, 2.462  
150 and 2.615 J/m<sup>2</sup>, respectively. Both the Pt (001) and Pt (011) have three adsorption sites, indicated by  
151 atop (A), bridge (B) and four-fold hollow (4F), while the Pt (111) has four sites indicated by atop (A),  
152 bridge (B), face-cubic centred (*fcc*) and hexagonal close packed (*hcp*). All the Pt atoms throughout this  
153 paper, is gold coloured, but for clarity the second layer atoms below the top surface are displayed in a  
154 lighter colour.



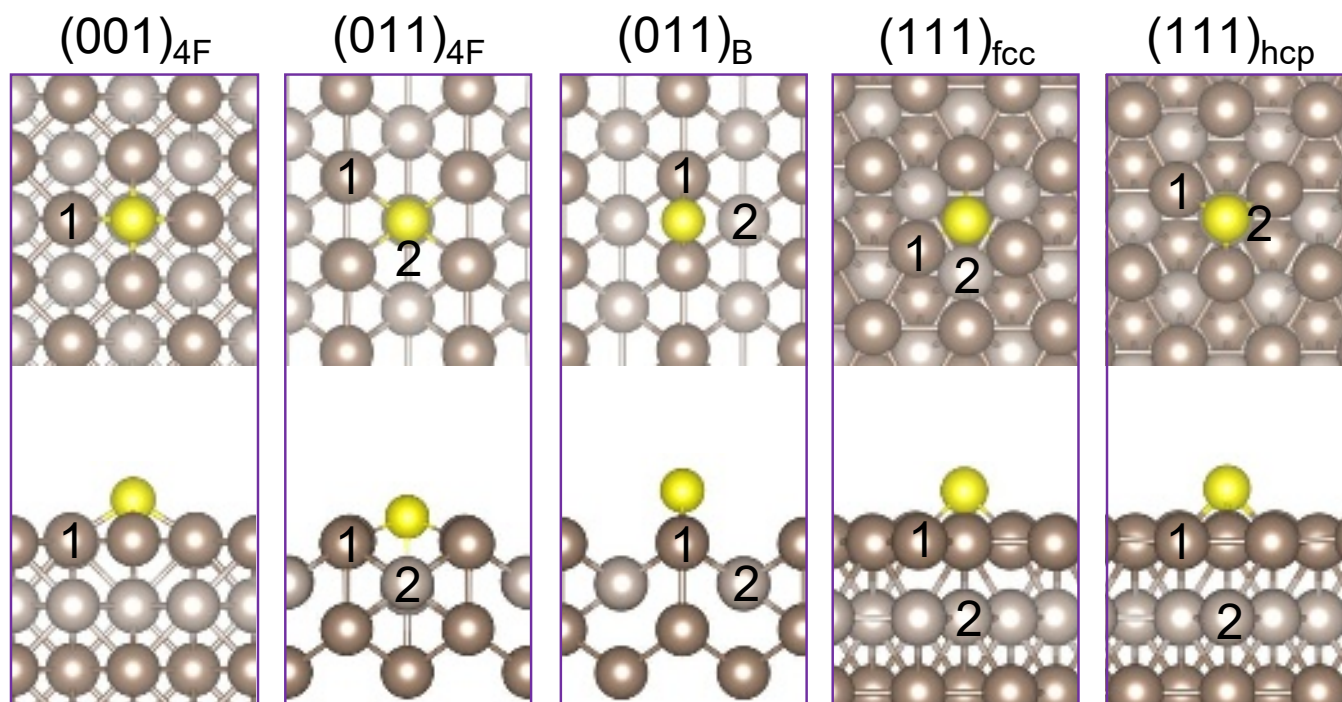
155

156 Figure 1 – Top views of the Pt (001), (011) and (111) surfaces, with the adsorption sites indicated as  
 157 four-fold hollow (4F), bridge (B) and atop (A), face-cubic centred (*fcc*) and hexagonal close packed (*hcp*).  
 158 All Pt atoms are gold in colour throughout the paper, with the second layer in a lighter colour to distinguish  
 159 between top layer and subsequent layer atoms.

160

### 161 3.2 S Adsorption and Surface Coverage

162 Only one atom of elemental sulphur (S) was considered for adsorption in all adsorption sites on all three  
 163 Pt surfaces. The most stable adsorptions are shown in Figure 2, with the adsorption energies ( $E_{\text{ads}}$ ),  
 164 charge transfer and bond distance ( $d$ ) of the adsorbed S on the Pt (001), (011) and (111) surfaces listed  
 165 in Table 1. The most stable adsorption with regard to adsorption energy was on the Pt (001) surface at  
 166  $-7.09$  eV, followed by both the Pt (011) and Pt (111) with adsorption energies ranging between  $-5.1$  and  
 167  $-5.5$  eV. Alfonso [79] also showed that the most stable S adsorption on the Pt (111) occurs in the *fcc*  
 168 site ( $-5.23$  eV) followed by the *hcp* site ( $-5.03$  eV). In both the Pt (001) and Pt (011) surfaces, the S atom  
 169 prefers the 4F hollow adsorption site, whereas on the (111) surface, both the *fcc* and *hcp* hollow is  
 170 preferred. Rodríguez and Santana [80] have shown that S adsorption is most stable on the  $(100)_{4F}$   
 171 surface ( $-5.16$  eV), followed by  $(111)_{fcc}$  surface ( $-4.63$  eV) and then the (110) surface ( $-4.37$  eV),  
 172 however in the B site rather than the 4F binding site. From the charge analysis in Table 1, the negative  
 173 values of  $\Delta q$  indicate charge transfer from the surface to the adsorbate, where most charge was  
 174 transferred to the  $(011)_{4F}$  site, followed by  $(111)_{hcp}$ ,  $(011)_B$ ,  $(011)_{4F}$  and  $(111)_{fcc}$ . Interestingly, in the of the  
 175  $(001)_{4F}$ ,  $(011)_B$  and  $(111)_{fcc}$  sites, S is surrounded by various Pt atoms in the surface, but none in the  
 176 second layer just below the S atom, whereas in the  $(011)_{4F}$  and  $(111)_{hcp}$  sites, a Pt atom in the second  
 177 layer is located below the S atom, contributing to the higher electron transfer observed (Table 1). The  
 178 adsorption energy for  $N_S = 1$  was calculated to be most favourable on the (001) surface, followed by the  
 179 (011) and (111) surfaces, which is the same trend as was found for  $H_2O$  and  $SO_2$  adsorption [46–48].



180

181 Figure 2 – Stable absorption sites of S on Pt (001), (011) and (111) surfaces. The atom colour yellow  
 182 denotes sulphur atoms. The numbers (1, 2) in the figure indicate the significant Pt atoms in the surface  
 183 (1) or in the second layer (2).

184

185 Table 1 – Adsorption energies ( $E_{\text{ads}}$ ), charge transfer and bond distance ( $d$ ) of the adsorbed S on the Pt  
 186 (001), (011) and (111) surfaces, with  $\theta_{(001)/(111)} = 0.11$ ,  $\theta_{(011)} = 0.06$ . The numbers (Pt<sub>1</sub>, Pt<sub>2</sub>) indicates the  
 187 significant Pt atoms in the surface or in the second layer, as shown in Figure 2..

		(001) <sub>4F</sub>	(011) <sub>4F</sub>	(011) <sub>B</sub>	(111) <sub>fcc</sub>	(111) <sub>hcp</sub>
d (Å)	$E_{\text{ads}}$ (eV)	-7.09	-5.47	-5.14	-5.47	-5.26
	$\Delta q$ (e)	-0.07	-0.25	-0.08	-0.06	-0.18
	S-Pt <sub>1</sub>	2.35	2.46	2.20	2.26	2.26
	S-Pt <sub>2</sub>	-	2.34	3.61	4.14	3.87

188

189 The most stable configurations ((001)<sub>4F</sub>, (011)<sub>4F</sub> and (111)<sub>fcc</sub>) were used to investigate surface coverage,  
 190 by increasing the number of adsorbed S atoms ( $N_{\text{SO}_x}$ ,  $x = 0$ ) on each Pt surface until a monolayer (ML)  
 191 was obtained. To obtain the lowest energy configurations, shown in Figure 3, various placements of  
 192 subsequent S atoms were considered. To determine if adsorption is still favoured as the surface coverage  
 193 increases, the average adsorption energy as a function of the surface coverage is shown in Figure 4(a),  
 194 whereas the sequential adsorption energy as a function of surface coverage is shown in Figure 4(b).



This is the author's peer reviewed, accepted manuscript. However, the online version of record will be different from this version once it has been copyedited and typeset.  
PLEASE CITE THIS ARTICLE AS DOI:10.1063/5.0043501

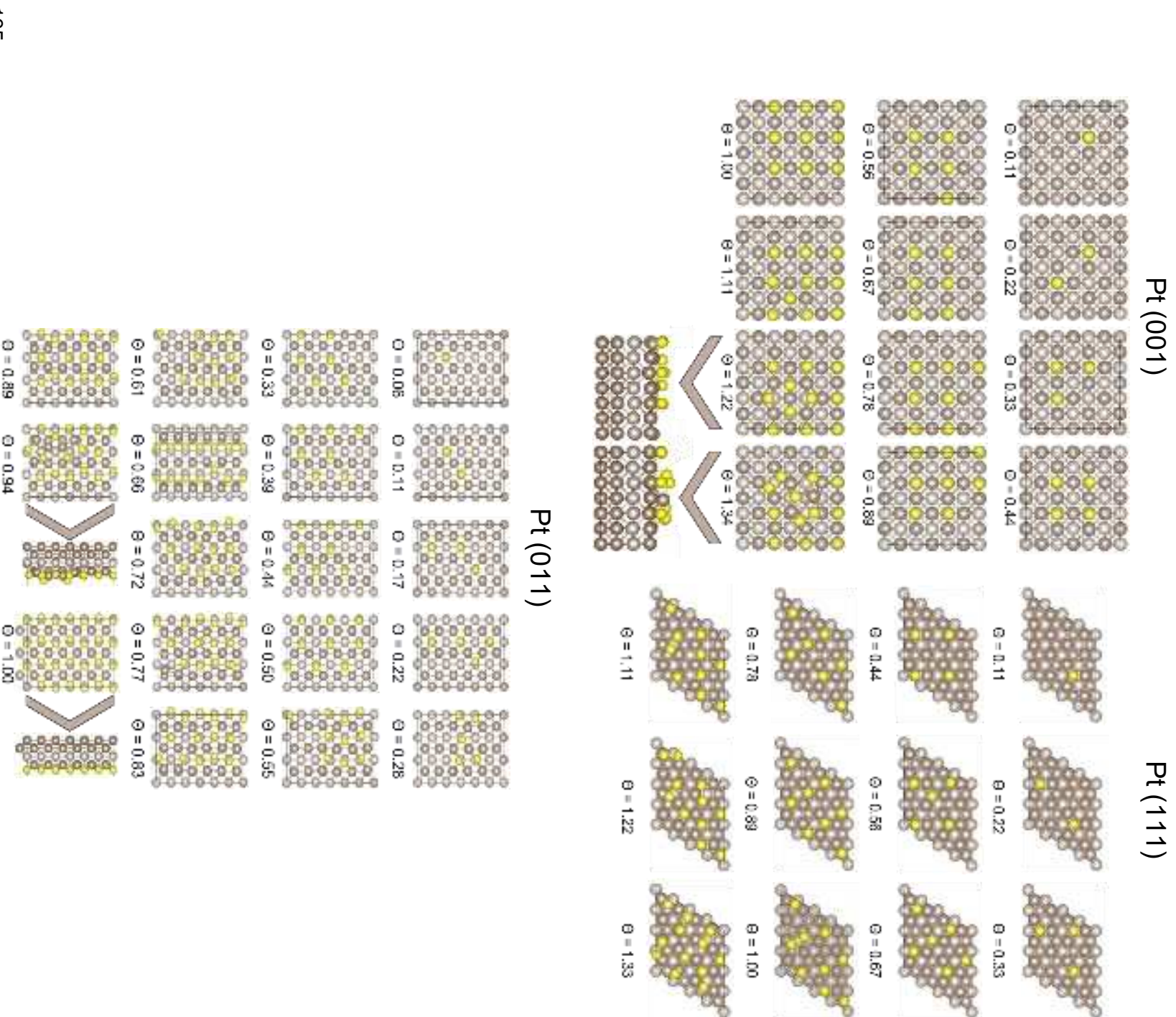
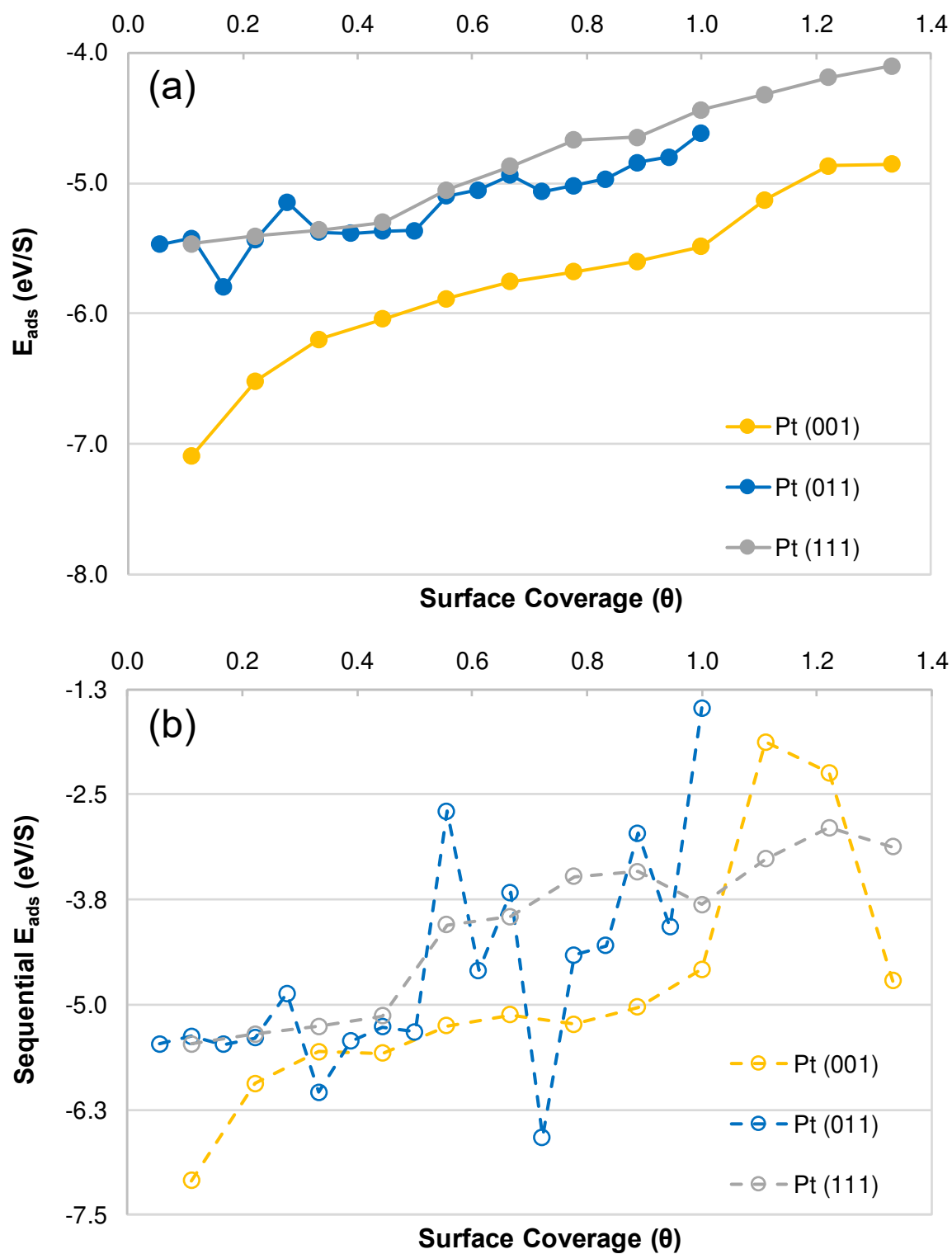


Figure 3 – Increased adsorption coverage of S on Pt (001), (011) and (111) surfaces.

This is the author's peer reviewed, accepted manuscript. However, the online version of record will be different from this version once it has been copyedited and typeset.  
PLEASE CITE THIS ARTICLE AS DOI:10.1063/1.50043501



198

199 Figure 4 – Average (a) and sequential (b) adsorption energies ( $E_{\text{ads}}$ ) as a function of the S surface  
200 coverage ( $\theta$ ) on the Pt (001), (011) and (111) surfaces.

201

202 Not surprisingly, more S atoms could be adsorbed onto the Pt surfaces, than H<sub>2</sub>O [46] or SO<sub>2</sub> [47]  
203 molecules. On the (001) surface, as the surface coverage increases up to  $\theta = 1.11$ , the mode of  
204 adsorption remained the same; no recombination occurs during the geometry optimisations. However,  
205 as the coverage increased to  $\theta = 1.22$ , the surface became 'crowded' and the S atoms are no longer  
206 perfectly adsorbed in the 4F hollow. At  $\theta = 1.34$ , the S atoms surrounded one of the surface Pt atoms  
207 and displaced it out of the surface plane and two S<sub>2</sub> molecules formed on the surface. This behaviour  
208 confirms experimental reports [9] that Pt electrodes are poisoned and in extreme cases delamination of  
209 Pt occurs when S deposition is detected on the surface. The average adsorption energy is calculated as  
210 a function of the surface coverage of S, i.e. the total adsorption energy divided by the maximum number  
211 of binding sites, i.e. 9, 18, 9 for the (001), (011) and (111) surface, respectively. Figure 4(a) shows that  
212 the same trend is observed as in previous studies on H<sub>2</sub>O and SO<sub>2</sub> adsorption, where the  $E_{\text{ads}}$  decreases  
213 with increased  $\theta$ . The sequential adsorption also shows that up to  $\theta = 1.11$ ,  $E_{\text{ads}}$  decrease. However, at  
214 higher coverages  $\theta \geq 1.22$ , the  $E_{\text{ads}}$  increases due the formation of S<sub>2</sub>. Also, as the Pt is displaced into  
215 the vacuum, the surface becomes more unstable and less active, which can also cause the  $E_{\text{ads}}$  to  
216 increase.

217 On the (011) surface, when adsorption was increased to  $\theta = 1$ , no S recombination or Pt delamination  
218 occurred. At  $\theta > 1$ , a second layer of S started to form, showing that the (011) surface was less reactive.  
219 Similar to the (001) surface, the average  $E_{\text{ads}}$  decreases with increasing  $\theta$ , but the sequential  $E_{\text{ads}}$  did not  
220 show a clear trend.

221 The Pt (111) surface showed no reactivity or delamination up to  $\theta = 0.89$ . However, when all 9 *fcc* sites  
222 were filled ( $\theta = 1$ ), S started to adsorb onto the *hcp* sites, resulting in the formation of S<sub>2</sub>. More pairs of  
223 S<sub>2</sub> formed as the S adsorption continued up to  $\theta = 1.33$ . Higher coverage was not obtained, however, as  
224 a second layer started forming. Due to the formation of S<sub>2</sub>, not all the S atoms were adsorbed onto the  
225 *fcc* sites and no Pt displacement was observed. Similar to the other two surfaces, the  $E_{\text{ads}}$  increased as  
226  $\theta$  increased, which was also observed in the sequential  $E_{\text{ads}}$  data. With the formation of the S<sub>2</sub> molecules,  
227  $E_{\text{ads}}$  increased slightly.

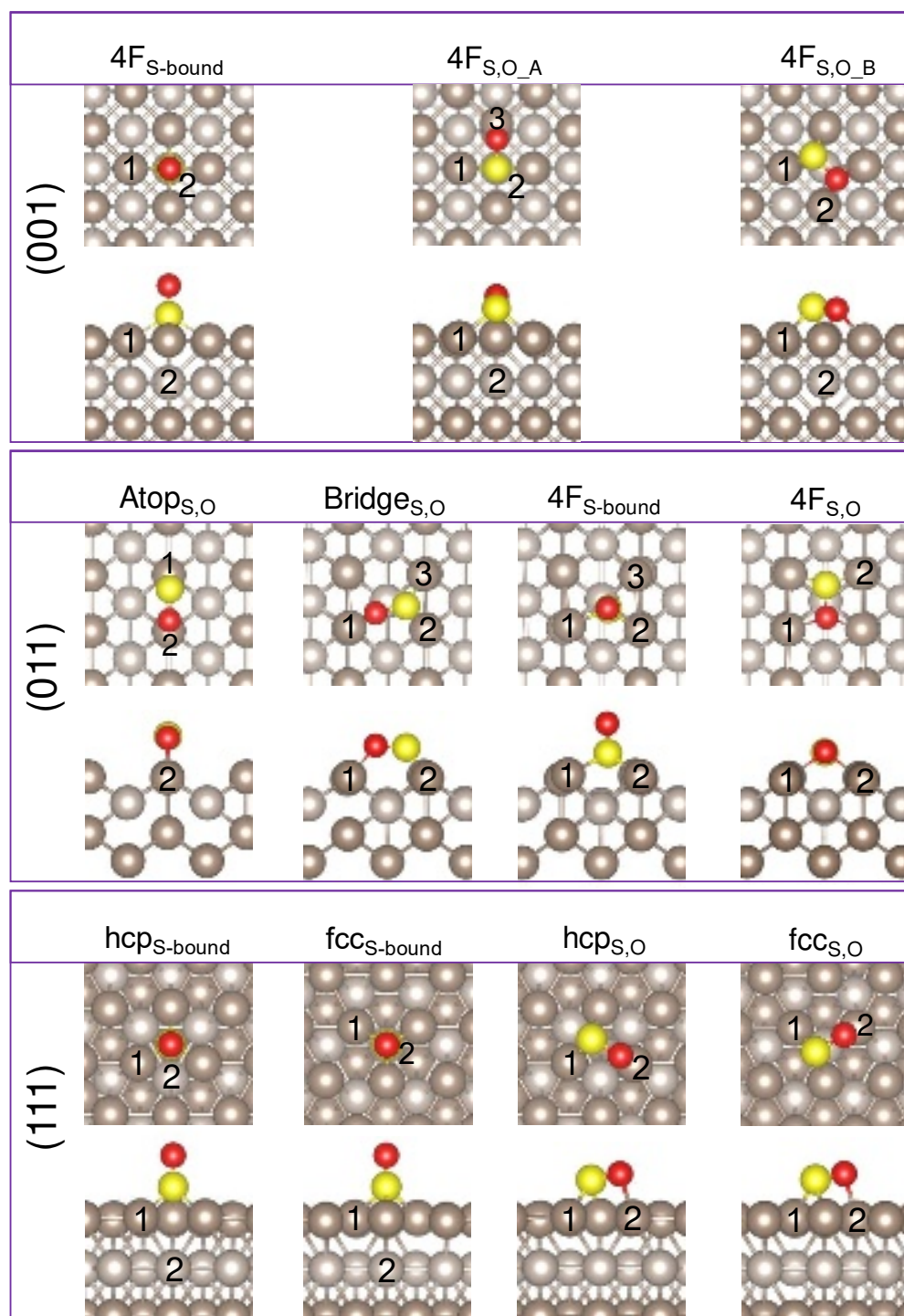
228 Comparing the increase in coverage on all three Pt surfaces, it was seen that the highest coverage of S  
229 was obtained on the (001) and (111) surfaces, followed by the (011) surface. Also, both the (001) and  
230 (111) surfaces were reactive towards the formation of S<sub>2</sub> and Pt degradation.

231

### 232 3.3 SO Adsorption and Surface Coverage

233 Three modes of SO adsorption on the metallic surfaces have been investigated, including S-bound, O-  
234 bound and S,O-bound on all the adsorption sites shown in Figure 1. The most stable structures for the

235 SO adsorption on the Pt surface in terms of adsorption energy are shown in Figure 5. The correlating  
 236 adsorption energy, bond distances and angles and charge transfer of the adsorbed SO, with respect to  
 237 the Pt surfaces, are shown in Table 2.



238

239 Figure 5 – Stable absorption sites of SO on Pt (001), (011) and (111) surfaces. The atom colours yellow  
 240 and red denotes sulphur and oxygen atoms, respectively. The numbers (1, 2) in the figure indicate the  
 241 significant Pt atoms in the surface (1) or in the second layer (2).

242 Table 2 – Adsorption energies ( $E_{\text{ads}}$ ), bond distance (d) and angles ( $\angle$ ) of the adsorbed SO on the Pt (001), (011) and (111) surfaces, with the  
 243 relevant charge transfers ( $\Delta q$ ) following adsorption, with  $\theta_{(001)/(111)} = 0.11$ ,  $\theta_{(011)} = 0.06$ . The numbers (Pt<sub>1</sub>, Pt<sub>2</sub>) indicate the significant Pt atoms  
 244 n the surface or in the second layer shown in Figure 5.

		(001)			(011)				(111)			
		4F <sub>s</sub>	4F <sub>s,O_A</sub>	4F <sub>s,O_B</sub>	Atop <sub>s,O</sub>	Bridges <sub>s,O</sub>	4F <sub>s</sub>	4F <sub>s,O</sub>	hcp <sub>s</sub>	fcc <sub>s</sub>	hcp <sub>s,O</sub>	fcc <sub>s,O</sub>
d (Å)	$E_{\text{ads}}$ (eV)	-5.10	-4.83	-4.12	-3.01	-3.56	-3.17	-3.57	-3.39	-3.25	-3.19	-3.10
	$\Delta q$ (e)	-0.07	-0.21	-0.41	-0.17	-0.21	-0.07	-0.26	-0.17	-0.12	-0.25	-0.23
$\angle$ (°)	S-Pt <sub>1</sub>	2.33	2.32	2.23	2.15	3.35, 2.30(Pt <sub>3</sub> )	2.38, 2.43(Pt <sub>3</sub> )	3.19	2.23	2.23	2.26	2.26
	S-Pt <sub>2</sub>	3.35	3.58	3.10	2.97	2.21	2.25	2.26	4.10	3.84	2.85	2.85
	O-Pt	3.35 (Pt <sub>1</sub> )	2.10 (Pt <sub>3</sub> )	2.19 (Pt <sub>2</sub> )	2.06 (Pt <sub>2</sub> )	2.15 (Pt <sub>1</sub> )	2.31 (Pt <sub>1</sub> )	2.40 (Pt <sub>1</sub> )	3.35 (Pt <sub>1</sub> )	3.37 (Pt <sub>1</sub> )	2.15 (Pt <sub>2</sub> )	2.18 (Pt <sub>2</sub> )
	S-O	1.47	1.60	1.67	1.58	1.57	1.48	1.63	1.46	1.46	1.56	1.56
	O-S-Pt	121.8 (Pt <sub>1</sub> )	103.12 (Pt <sub>1</sub> )	103.6 (Pt <sub>1</sub> )	106.1 (Pt <sub>1</sub> )	112.1 (Pt <sub>2</sub> )	115.9 (Pt <sub>1</sub> )	104.3 (Pt <sub>2</sub> )	129.2 (Pt <sub>1</sub> )	130.8 (Pt <sub>1</sub> )	106.8 (Pt <sub>1</sub> )	105.2 (Pt <sub>1</sub> )
	SO- surf <sub>L</sub>	89.7	21.02	79.6	16.1	14.9	2.7	91.6	92.6	93.4	30.4	32.2

245

246

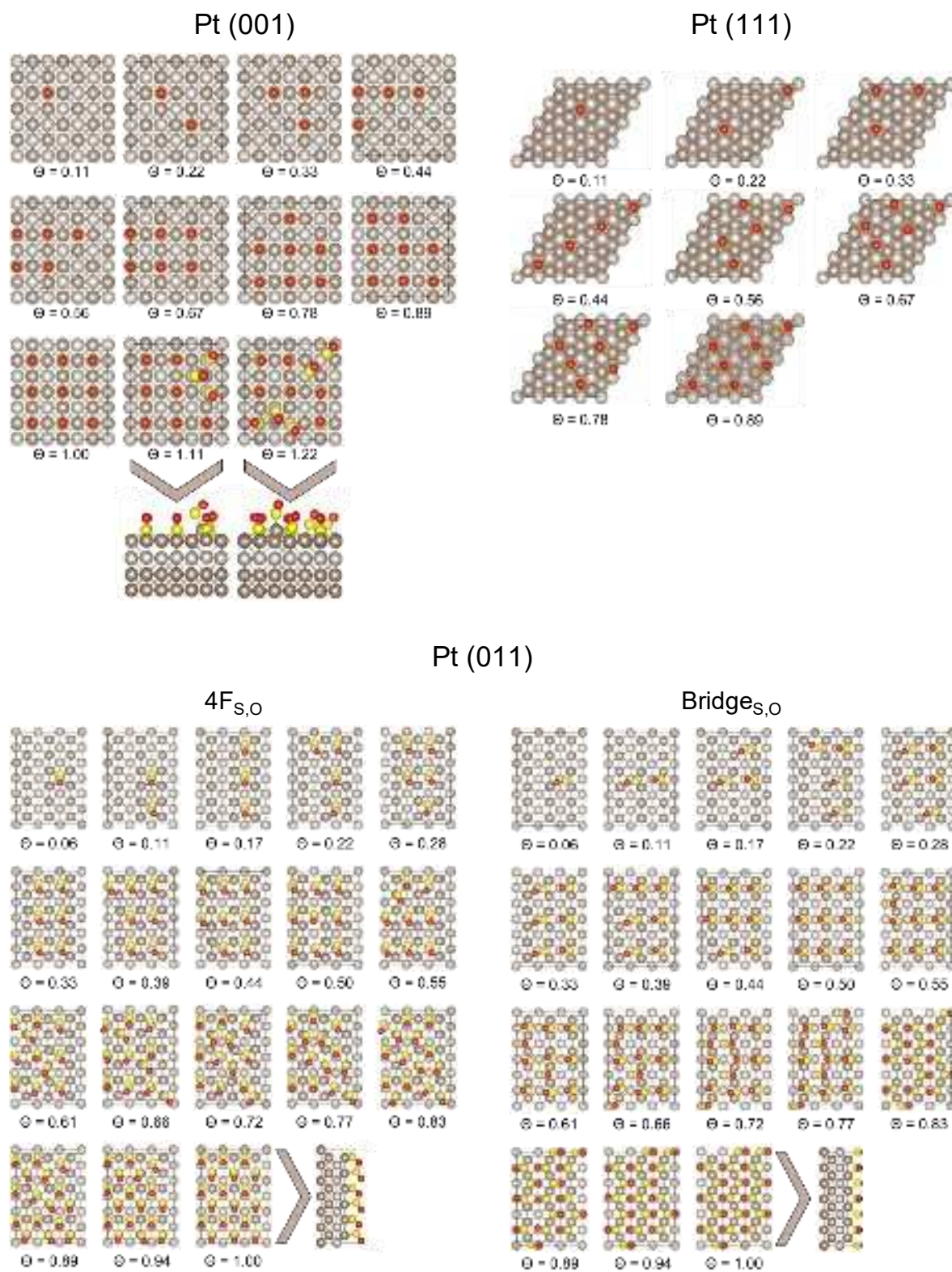
247 Three stable SO adsorption configurations were obtained for the (001) surface. All three were on the 4F  
248 binding site, with the highest adsorption energy achieved where S was bound to the Pt surface and the  
249 O directed away, i.e.  $4F_{S\text{-bound}}$ , followed by two configurations where both S and O were bound to Pt. In  
250 the first configuration,  $4F_{S,O\_A}$ , the S atom is bound to two Pt atoms on opposite sides of the 4F hollow,  
251 with the O atom bound to a third Pt atom; in the second configuration,  $4F_{S,O\_B}$ , both the S and O atoms  
252 are bound to two Pt atoms on either side of the 4F hollow, as shown in Figure 5. We note that the charge  
253 transfer is lowest ( $-0.07 e^-$ ) when only one S is bound to the Pt surface, followed by the tri-bound  $4F_{S,O\_A}$   
254 ( $-0.21 e^-$ ) and the tetra-bound  $4F_{S,O\_A}$  ( $-0.41 e^-$ ) configurations. When comparing the S-O bond length,  
255 it can be seen that the adsorption configuration can cause a deviation of up to  $0.2 \text{ \AA}$  from the  
256 experimentally measured S-O bond length of  $1.44 \text{ \AA}$  [81], which correlates with the  $4F_{S\text{-bound}}$  structure.  
257 This shows that the bond lengths and charge transfer are dependent on the bond order and type of bonds  
258 formed during adsorption. [82]

259 On the Pt (011) surface four stable adsorption configurations were observed, one being S-bound and  
260 three S,O-bound. Energetically, the most stable is the tetra-bound configuration  $4F_{S,O}$ , within a 4F hollow,  
261 following the groove on the (011) surface, closely followed by the tri-bound  $\text{Bridge}_{S,O}$  where SO is again  
262 in the 4F hollow, but across the (011) groove. The third most stable configuration is the  $4F_{S\text{-bound}}$ , with a  
263 bidentate S offset from the 4F hollow, followed by the fourth configuration,  $\text{Atop}_{S,O}$  where S,O forms a  
264 bidentate configuration on the ridge of the (011) surface between two Pt atoms, as shown in Figure 5.  
265 Similar to the (001) surface, the charge transfer is dependent on the bond orders  $4F_{S,O}$  (4) >  $\text{Bridge}_{S,O}$  (3)  
266 >  $4F_{S\text{-bound}}$  (2) >  $\text{Atop}_{S,O}$  (2). As on the (001) surface, the S-O bond length of  $4F_{S\text{-bound}}$  correlates with the  
267 free S-O bond length, but in the other cases deviates by up to  $0.15 \text{ \AA}$ , [81] depending on the adsorption  
268 configuration.

269 The (111) surface achieved four stable adsorption configurations, either with a S,O-bonded or S-bound  
270 geometry on both the *fcc* and *hcp* binding sites, i.e.  $\text{fcc}_{S,O}$ ,  $\text{fcc}_{S\text{-bound}}$ ,  $\text{hcp}_{S,O}$  and  $\text{hcp}_{S\text{-bound}}$ , respectively.  
271 Similar to the (001) surface, the adsorption energy was the highest for the S-bound configurations,  $\text{hcp}_{S\text{-bound}}$   
272  $\text{bound} > \text{fcc}_{S\text{-bound}}$ , followed by the S,O-bound configurations,  $\text{hcp}_{S,O} > \text{fcc}_{S,O}$ . Similar to the trends observed  
273 on both the (001) and (011) surfaces, the charge transfer increased as the bond order increased,  $\text{fcc}_{S\text{-bound}}$   
274  $\text{bound} < \text{hcp}_{S\text{-bound}} < \text{fcc}_{S,O} < \text{hcp}_{S,O}$ . As on the (011) surface, the S-O bond length of S-bound configurations  
275 ( $\text{fcc}_{S\text{-bound}}$  and  $\text{hcp}_{S\text{-bound}}$ ) correlates with the free S-O bond length, but it is elongated by  $0.1 \text{ \AA}$  in the S,O-  
276 bound configurations ( $\text{fcc}_{S,O}$  and  $\text{hcp}_{S,O}$ ).

277 Similar to the adsorption of S,  $\text{H}_2\text{O}$  and  $\text{SO}_2$ , the adsorption energy for  $N_{SO} = 1$  was calculated to be most  
278 favourable on the (001) surface, followed by the (011) and (111) surfaces [46–48]. The most stable SO  
279 configurations on all three Pt surfaces were used to investigate the effect of surface coverage. However,

280 on the (011) surface, the  $4F_{s,o}$  and  $Bridge_{s,o}$  had similar adsorption energies, and thus, the four  
281 configurations considered included  $(001)_{4F_s}$ ,  $(011)_{4F_{s,o}}$ ,  $(011)_{B_{s,o}}$  and  $(111)_{hcp_s}$ , shown in Figure 6.



282

283 Figure 6 – Increased SO coverage on the Pt (001), (011) and (111) surfaces.

284 As with the adsorption of S, the number of adsorbed SO molecules ( $N_{SO_x}, x = 1$ ) is increased on each Pt  
285 surface, until a monolayer was obtained. Figure 7 shows the corresponding surface coverage as a  
286 function of both adsorption energy (a) and sequential adsorption energy (b). As with the adsorption of  
287 elemental S, it can be seen that on the Pt (001) the  $E_{ads}$  decreases steadily as the surface coverage is  
288 increased, in correlation with the sequential  $E_{ads}$  up to  $\theta = 1$ . At this stage, all the 4F hollow adsorption  
289 sites are occupied and very stable. However at  $\theta = 1.11$ , one of the SO molecules is bound atop a Pt  
290 atom which is pulled out from the surface, causing the sequential  $E_{ads}$  to decrease. When a second SO  
291 molecule was added in the atop site, again a Pt atom was displaced from the surface, indicating that it is  
292 not only elemental S which causes Pt delamination in a catalytic environment, but that the presence of  
293 SO can also cause surface destabilisation and possibly catalyst degradation. At  $\theta > 1.22$ , a second layer  
294 of SO started to form, but there was no evidence that SO molecules reacted with each other.

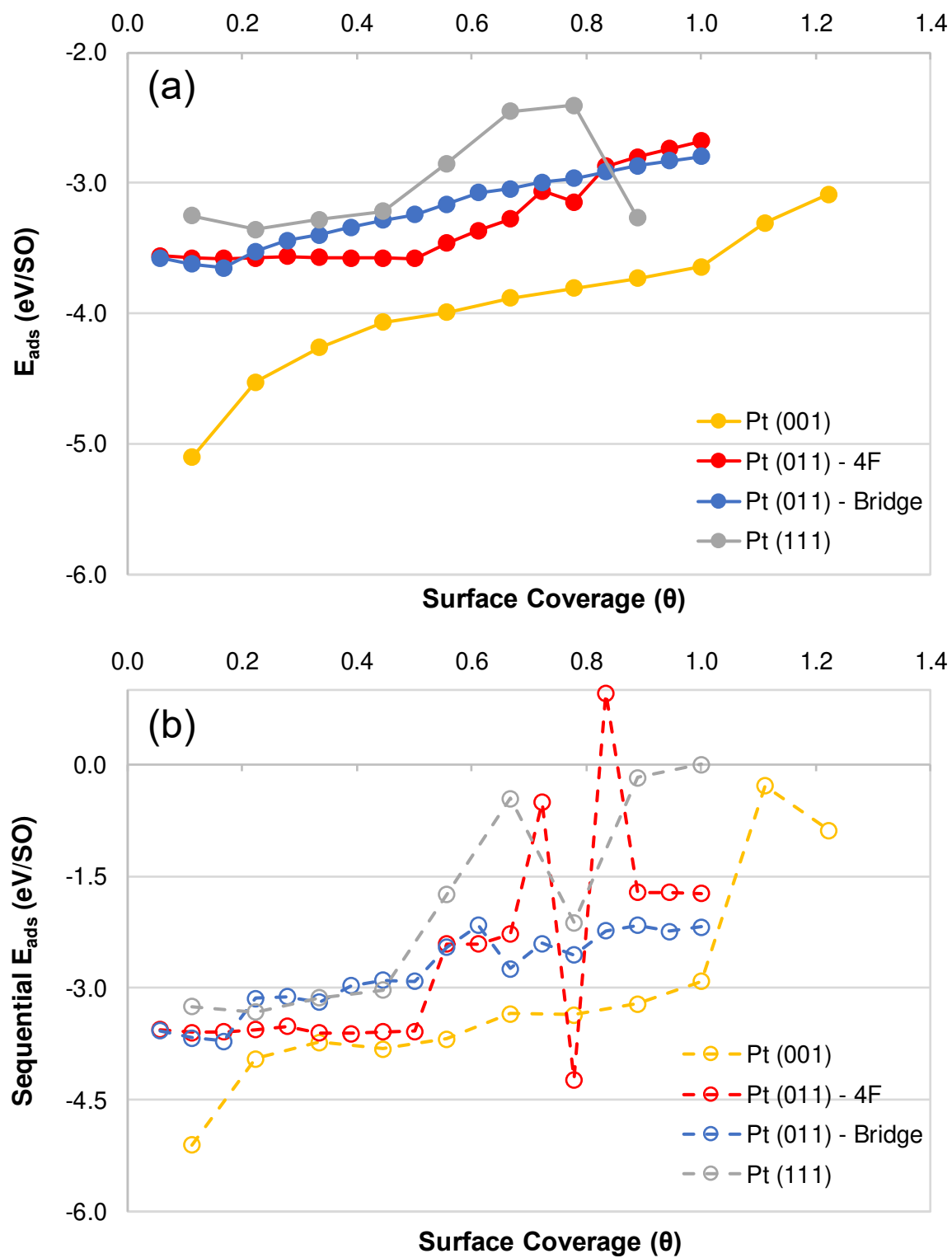
295 As on the (001) surface, on the Pt (011) surface  $E_{ads}$  decreased linearly as  $\theta$  increased for both the  $4F_{S,O}$   
296 and  $Bridge_{S,O}$  adsorption configurations until full coverage ( $\theta = 1$ ) was obtained. Comparing the sequential  
297  $E_{ads}$  for both these adsorption, it can be seen that in the  $4F_{S,O}$  case  $E_{ads}$  plateaus up to a coverage of  $\theta =$   
298 0.55. At coverages  $0.55 < \theta < 0.73$ , the surface becomes crowded, causing the sequential  $E_{ads}$  to  
299 decrease significantly, due to a change in SO adsorption. However, at  $\theta = 0.77$  the sequential  $E_{ads}$   
300 increased sharply, due to all the SO molecules aligning in a similar fashion to the single SO adsorption  
301 configuration. At  $\theta = 1$ , all the adsorption sites are occupied and stable. Coverages of  $\theta > 1$  were not  
302 observed, as a second layer started to form. Similar to the (001) surface, no reaction between sequential  
303 SO molecules were observed on the Pt (011) surface. In the case of the increased surface coverage of  
304  $Bridge_{S,O}$  both the  $E_{ads}$  and sequential  $E_{ads}$  decreased as  $N_{SO}$  increased. In this case the adsorption  
305 configuration stayed very similar to the single SO adsorption. Higher coverage than  $\theta > 1$  was not  
306 obtained as a second layer started to form. Again, no reaction between the SO molecules was observed.

307 Similar to the other surfaces, the (111) surface showed a steady decrease in  $E_{ads}$  and sequential  $E_{ads}$  as  
308  $\theta$  increased. At  $\theta = 1$ , all hcp sites were occupied by SO, but as an additional SO was placed on an *fcc*  
309 site, a second SO layer started to form. As with the other surfaces, the subsequent addition of SO  
310 molecules did not lead to additional reactions.

311 Comparing the increased coverage on all three Pt surfaces, it was seen that the highest coverage of SO  
312 was achieved on the (001) surface, followed by the (011) and then (111) surfaces.



This is the author's peer reviewed, accepted manuscript. However, the online version of record will be different from this version once it has been copyedited and typeset.  
PLEASE CITE THIS ARTICLE AS DOI:10.1063/1.50043501



313

314 Figure 7 – Average (a) and sequential (b) adsorption energies ( $E_{\text{ads}}$ ) as a function of the SO surface  
315 coverage ( $\text{nm}^{-2}$  Pt) on the Pt (001), (011) and (111) surfaces.

316

317 **3.4 SO<sub>3</sub> Adsorption and Surface Coverage**

318 The literature has shown [19] that five modes of SO<sub>3</sub> adsorption are possible and all were considered in  
319 this work, including (i) planar O,O,O, where all four atoms are parallel to the surface, (ii) S,O,O, where  
320 only two S-O interact with the surface, (iii) O,O where only two of the O atoms interact, (iv) S,O where  
321 one S-O bond interact with the surface and the other two O atoms are directed away from the surface  
322 and (v) where only one O atom interacts with the surface. All five modes were investigated in the various  
323 adsorption sites shown in Figure 1. The most stable structures found for the adsorption of SO<sub>3</sub> onto the  
324 Pt surface are shown in Figure 8, with the adsorption energies, charge transfer, bond distances and  
325 angles of the adsorbed SO<sub>3</sub> with respect to the Pt surfaces listed in Table 3.

326 On the (001) surface, two stable configurations were observed, the most stable being 4F<sub>S-bound</sub>, where  
327 the S atom is bound within a 4F hollow, and two O atoms bind to two Pt atoms of the 4F hollow with the  
328 third O atom directed towards the vacuum. The second adsorption mode is Atop<sub>O,O,O</sub>, where again the S  
329 atom is in the 4F hollow and all three O atoms are bound atop a Pt atom of the 4F hollow. The literature  
330 has shown that on the  $\alpha$ -Fe<sub>2</sub>O<sub>3</sub> (001) surface [83], an O,O-bridge formed on the surface with a binding  
331 energy between -2.27 and -2.46 eV, depending on whether the bridge formed over a Fe-O or Fe-Fe  
332 binding site, respectively. Similar to the adsorption of SO on (001), the charge transfer increased as the  
333 bond order increased. The free SO<sub>3</sub> molecule showed an average S-O bond length of 1.47 Å and an O-  
334 S-O bond angle of 120°, which correlates with the free S-O(1) bond length in the 4F<sub>S-bound</sub> configuration.  
335 In both 4F<sub>S-bound</sub> and Atop<sub>O,O,O</sub>, the Pt-bound S-O bonds are stretched on average by 0.1 Å. In the 4F<sub>S-</sub>  
336 bound configuration, the planar SO<sub>3</sub> changed to a nearly tetrahedral configuration, causing the O-S-O bond  
337 angles to decrease. Also in the Atop<sub>O,O,O</sub> configuration, with the O atoms bound atop the Pt atoms, the S  
338 atom is pushed slightly out of plane, decreasing the O-S-O bond angles, which confirms a tetrahedral  
339 configuration and indicates that SO<sub>3</sub> is chemisorbed onto the (001) surface.

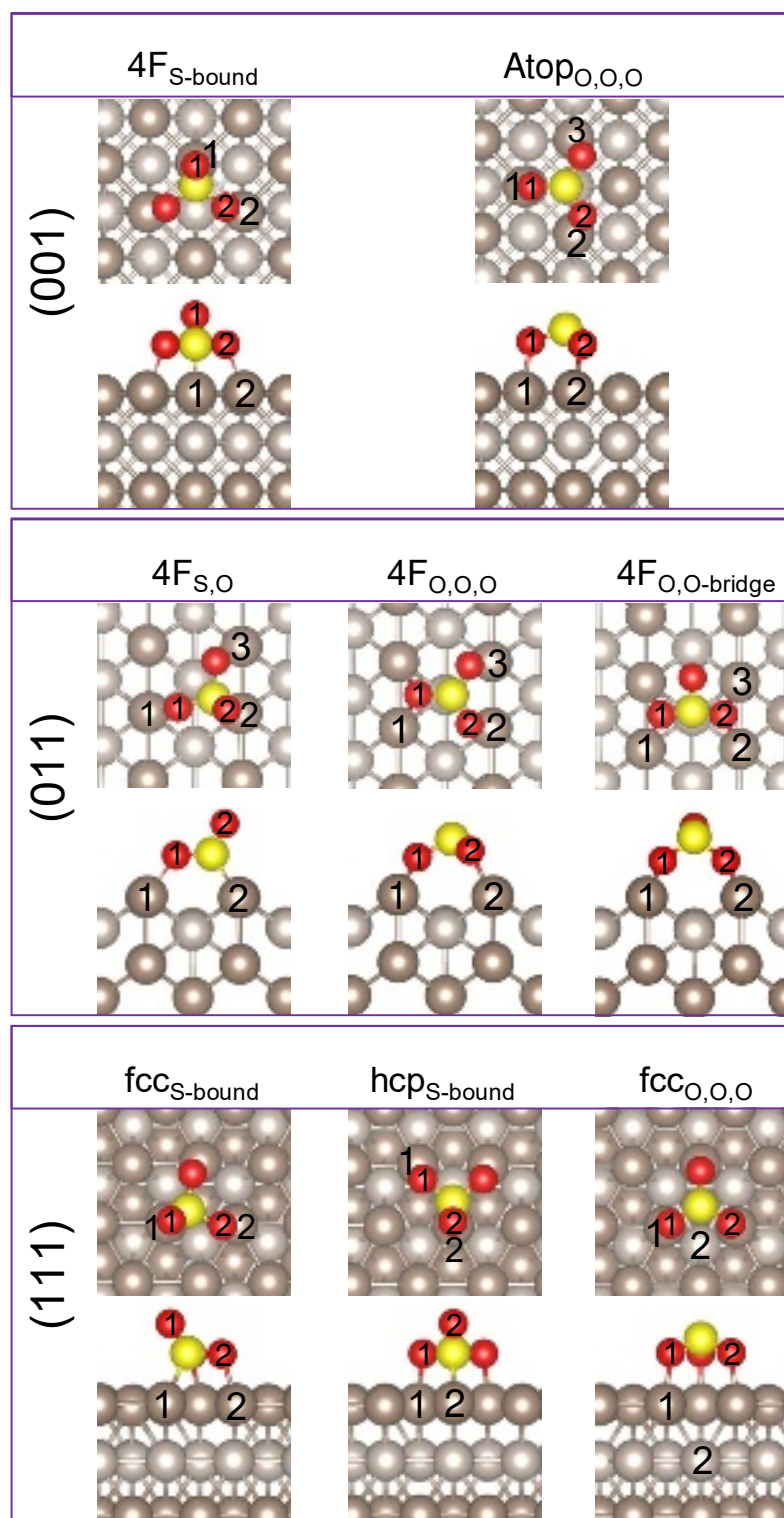
340 On the (011) surface, three stable adsorption modes were observed, 4F<sub>S,O</sub>, 4F<sub>O,O,O</sub> and 4F<sub>O,O-bridge</sub>. In the  
341 first configuration (4F<sub>S,O</sub>), the S atom is bound to one Pt atom on the ridge, one S-O(1) formed a bridge  
342 across the (011) ridge and the other S-O(3) formed a bridge on the (011) ridge and oxygen O(2) is  
343 directed towards the vacuum. The second stable configuration (4F<sub>O,O,O</sub>), S was over the 4F hollow, with  
344 all three O atoms bound to the Pt atoms of the 4F hollow, forming two S-O bridges across the (011) ridge.  
345 Similarly, in the third stable configuration (4F<sub>O,O-bridge</sub>) S was over the 4F hollow forming two S-O bridges  
346 across the (011) ridge, with O(3) directed along the groove of the (011) surface. It has been shown [83]  
347 on the  $\alpha$ -Fe<sub>2</sub>O<sub>3</sub> (001) surface, that Fe-O-Fe binding causes ridges and valleys similar to the (011) surface  
348 and on these Fe-O-Fe binding site, SO<sub>3</sub> forms a stable O,O-bridge across the surface, similar to our  
349 4F<sub>O,O-bridge</sub> configuration, with a binding energy of -2.27 eV.

350

This is the author's peer reviewed, accepted manuscript. However, the online version of record will be different from this version once it has been copyedited and typeset.  
PLEASE CITE THIS ARTICLE AS DOI:10.1063/1.50043501

351

352 Figure 8 – Stable absorption sites of  $\text{SO}_3$  on Pt (001), (011) and (111) surfaces. The atom colours yellow  
353 and red denotes sulphur and oxygen atoms, respectively. The numbers (1, 2) in the figure indicate the  
354 significant Pt or oxygen atoms in the surface (1) or in the second layer (2).  
355



356 Table 3 – Adsorption energies ( $E_{\text{ads}}$ ), bond distance (d) and angles ( $\angle$ ) of the adsorbed  $\text{SO}_3$  on the Pt (001), (011) and (111) surfaces, with the  
 357 relevant charge transfers ( $\Delta q$ ) following adsorption, with  $\theta_{(001)/(111)} = 0.11$ ,  $\theta_{(011)} = 0.06$ . The numbers (Pt<sub>1</sub>, Pt<sub>2</sub>, O<sub>1</sub>, O<sub>2</sub>, O<sub>3</sub>) indicate the significant  
 358 Pt and O atoms shown in Figure 8.

		(001)		(011)			(111)		
		4F <sub>s</sub>	Atop <sub>o,o,o</sub>	4F <sub>s,o,o</sub>	4F <sub>o,o,o</sub>	4F <sub>o,o-bridge</sub>	fcc_s	hcp_s	fcc_o,o,o
d (Å)	$E_{\text{ads}}$ (eV)	-3.38	-2.95	-2.68	-2.18	-1.39	-1.83	-1.79	-1.59
	$\Delta q$ (e)	-0.60	-0.84	-0.64	-0.86	-0.88	-0.58	-0.57	-0.83
	S-Pt <sub>1</sub>	2.23	3.12	3.26	3.50	3.55	2.27	2.94	3.16
	S-Pt <sub>2</sub>	3.03	3.27	2.23	3.22	3.55	2.95	2.26	3.16
	O <sub>1</sub> -Pt <sub>1</sub>	3.20	2.10	2.08	2.24	2.18	3.22	2.14	2.11
	O <sub>2</sub> -Pt <sub>2</sub>	2.10	2.11	3.14	2.10	2.18	2.12	3.23	2.11
	S-O <sub>1</sub>	1.44	1.54	1.55	1.62	1.64	1.44	1.54	1.55
	S-O <sub>2</sub>	1.55	1.56	1.45	1.53	1.64	1.54	1.44	1.54
$\angle$ (°)	O <sub>1</sub> -S-O <sub>2</sub>	110.2	106.8	108.0	106.6	105.8	111.1	111.1	107.2
	O <sub>2</sub> -S-O <sub>3</sub>	107.5	107.6	110.9	108.9	105.2	106.6	107.1	107.2

359

360

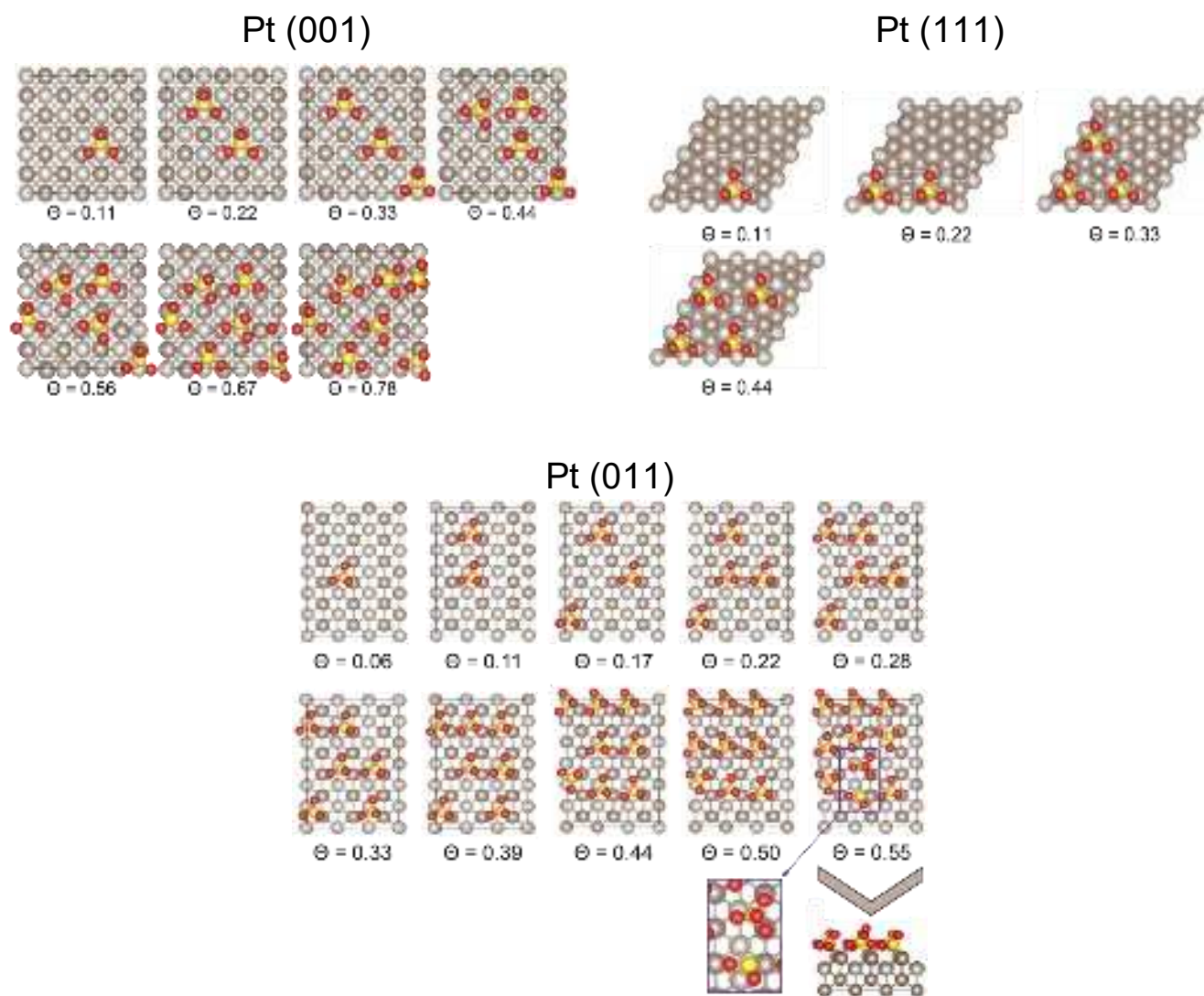
361 The charge transfer between  $\text{SO}_3$  and the (011) Pt surface did not follow the same bond order trend as  
362 observed for the other adsorptions. Interestingly, more electrons were transferred when either just two or  
363 all three O atoms were bound to the Pt surface ( $4F_{\text{O,O-bridge}}$  and  $4F_{\text{O,O,O}}$ , respectively), compared to when  
364 two O and one S atom were bound ( $4F_{\text{S,O}}$ ). As observed on the (001) surface, the bound  $\text{SO}_3$   
365 configuration changes to a tetrahedral mode, elongating the bound S-O bonds and decreasing the O-S-  
366 O bonds, again indicating that  $\text{SO}_3$  is chemisorbed onto the (011) surface.

367 On the (111) surface, three stable adsorption modes were observed, including  $\text{fcc}_{\text{S-bound}}$ ,  $\text{hcp}_{\text{S-bound}}$  and  
368  $\text{fcc}_{\text{O,O,O}}$ . The first two are similar, where S is bound over either an *fcc* or *hcp* hollow, with O atoms atop  
369 two of the Pt atoms of the hollow adsorption site. In the third adsorption configuration,  $\text{fcc}_{\text{O,O,O}}$ , S is again  
370 over an *fcc* hollow, with all three O atoms bound atop the surrounding Pt atoms. The  $\text{fcc}_{\text{S-bound}}$   
371 configuration is similar to our previously predicted  $\text{SO}_2$  adsorption on the (111) surface [47], which had  
372 an S,O-bonded geometry on the *fcc* binding site, with one S-O bond in the plane of the surface and the  
373 other oxygen directed away from the surface. Lin and co-workers [19] also showed that various  
374 adsorption configurations are possible on the (111) surface, with the  $\text{fcc}_{\text{S-bound}}$  being the most stable with  
375 a binding energy of 1.43 eV. They have also shown that the Pt bound S-O bond length is elongated (1.56  
376 Å), while the non-surface bound S-O is similar to the gas phase bond length of S-O (1.46 Å) with a  
377 decreased O-S-O bond angle ( $107^\circ$ ). Similar to the (001) surface, the charge transfer increased as the  
378 bond order increased, i.e.  $\text{fcc}_{\text{S-bound}} > \text{hcp}_{\text{S-bound}} > \text{fcc}_{\text{O,O,O}}$ . Chemisorption of  $\text{SO}_3$  occurred for all three  
379 configurations, similar to the (001) and (011) surfaces, the Pt bound S-O bond lengths increased and the  
380 O-S-O bond angles decreased.

381 Similar to the adsorption of S, SO,  $\text{H}_2\text{O}$  and  $\text{SO}_2$ , the adsorption energy for  $N_{\text{SO}_3} = 1$  was calculated to  
382 be most favourable on the (001) surface, followed by the (011) and (111) surfaces [46–48]. The most  
383 stable configurations –  $(001)_{4F_{\text{S}}}$ ,  $(011)_{4F_{\text{S,O}}}$  and  $(111)_{\text{fcc}_{\text{S}}}$  – were used to investigate surface coverage,  
384 by increasing the number of adsorbed  $\text{SO}_3$  molecules ( $N_{\text{SO}_3}, x = 3$ ) on each Pt surface, until a monolayer  
385 (ML) was obtained. To obtain the lowest energy configurations, shown in Figure 9, various placements  
386 of subsequent  $\text{SO}_3$  molecules were considered. To determine if adsorption is still favoured as the surface  
387 coverage increases, the average adsorption energy (Figure 10(a)) and the sequential adsorption energy  
388 Figure 10(b)) as a function of surface coverage were calculated.

389 As with the adsorption of elemental S and SO on the (001) surface, it can be seen that  $E_{\text{ads}}$  decreases  
390 steadily as the surface coverage increased and is also correlated with the sequential  $E_{\text{ads}}$  up to  $\theta = 0.67$ .  
391 The initial adsorption configurations up to  $\theta = 0.33$  show all the  $\text{SO}_3$  in the chosen adsorption mode and  
392 site of the isolated molecule. At  $\theta = 0.44$ , the surface becomes more crowded and one of the  $\text{SO}_3$   
393 molecules rotates slightly, but is still bound in the  $4F$  adsorption site, with two O atoms atop a Pt atom.  
394 This slight rotation of the  $\text{SO}_3$  molecule adsorption also occurs at higher coverages, possibly causing the

395 smaller adsorption energies. At the highest coverage ( $\theta = 0.78$ ), more distortions can be seen but no  
396 reaction occurred between the  $\text{SO}_3$  molecules.



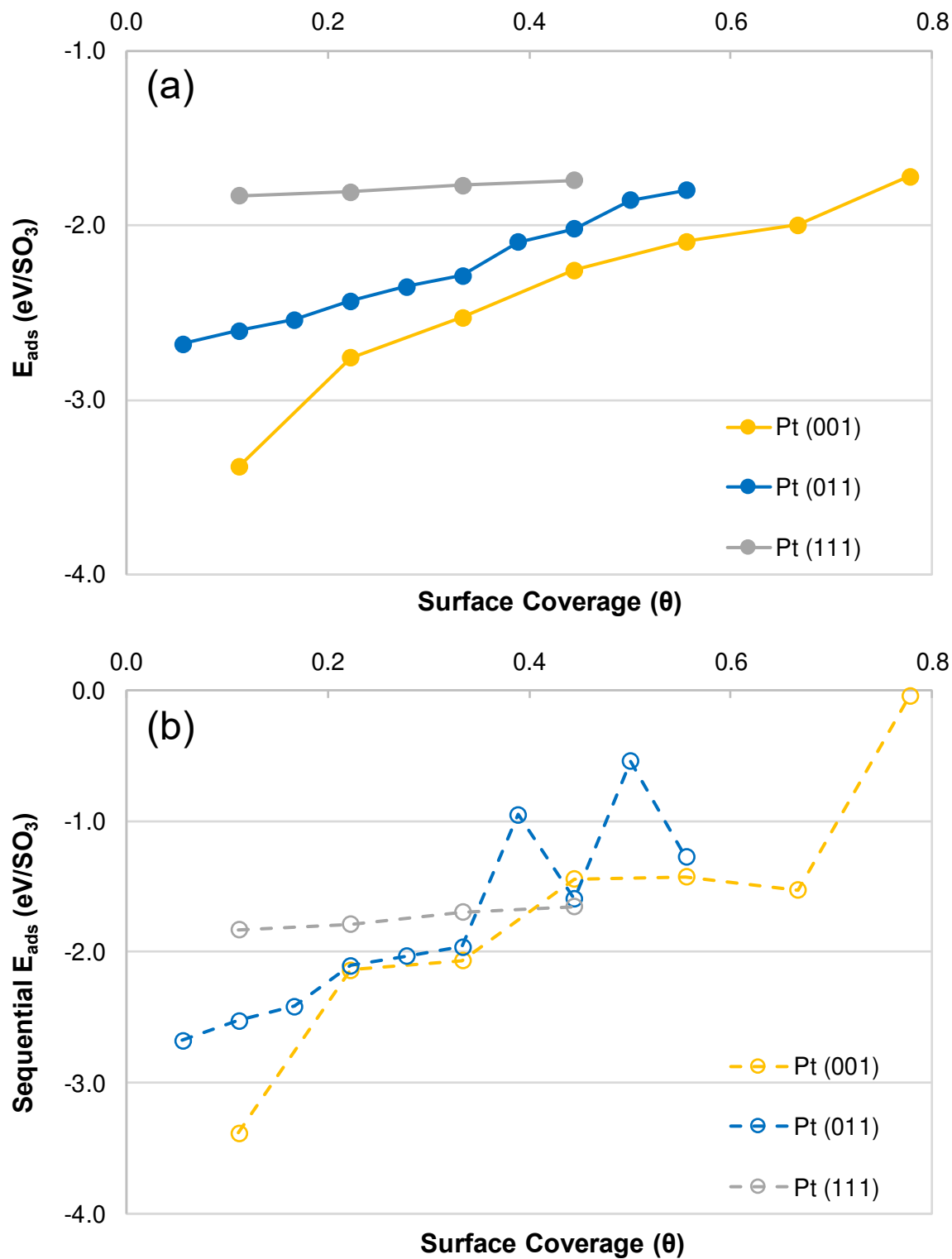
397

398 Figure 9 – Increased  $\text{SO}_3$  coverage on the Pt (001), (011) and (111) surfaces.

399

400 On the Pt (011) surface,  $E_{\text{ads}}$  again decreases steadily as  $\theta$  is increased. Furthermore, the sequential  
401  $E_{\text{ads}}$  also decreases with increased adsorption up to  $\theta = 0.39$ , but with the addition of another  $\text{SO}_3$  ( $\theta =$   
402  $0.44$ ), the surface becomes more crowded and a slight rotation occurs, causing the sequential  $E_{\text{ads}}$  to  
403 increase. This behaviour was repeated with an additional  $\text{SO}_3$  ( $\theta = 0.50$ ), causing all the  $\text{SO}_3$  to have the  
404 same orientation as with  $N_{\text{SO}_3} = 1$ , thereby increasing the surface strain and resulting in a smaller  
405 sequential  $E_{\text{ads}}$ . The adsorption of an additional  $\text{SO}_3$  at  $\theta = 0.55$  caused two  $\text{SO}_3$  molecules to react and  
406 form  $\text{SO}_4$  and  $\text{SO}_2$ . This secondary reaction caused the sequential  $E_{\text{ads}}$  to increase. No further  $\text{SO}_3$

407 molecules could be adsorbed as a secondary layer started to form, in addition to secondary reactions  
408 occurring.



409

410 Figure 10 – Average (a) and sequential (b) adsorption energies ( $E_{\text{ads}}$ ) as a function of the  $\text{SO}_3$  surface  
411 coverage ( $\text{nm}^{-2}$  Pt) on the Pt (001), (011) and (111) surfaces.

412 Similar to the increased coverage of  $\text{SO}_3$  on the (001) and (011) surfaces, both the  $E_{\text{ads}}$  and sequential  
413  $E_{\text{ads}}$  decreased with increased  $\theta$ . Coverages of  $\theta > 0.44$  were not obtained, as this caused not only  
414 secondary layers to form, but also the secondary reaction ( $2 \text{SO}_3 \rightarrow \text{SO}_2 + \text{SO}_4$ ) to occur, as observed  
415 on the (011) surface.

416 When we compare the increased coverages of  $\text{SO}_3$  on all three Pt surfaces, we observe that similar to  
417 the SO coverages, the highest coverage was achieved on the (001) surface, followed by the (011) and  
418 then (111) surfaces. The (011) surface was the most reactive towards secondary reactions between co-  
419 adsorbed  $\text{SO}_3$  molecules, followed by the (111) surface.

420

### 421 3.5 Thermodynamic Influence on Adsorption

422 The HyS cycle is operated at 1 atm (1.103 bar) and 350 to 400 K. Phase diagrams have therefore been  
423 constructed to determine the effect of temperature and pressure on the surface coverage of S, SO and  
424  $\text{SO}_3$ . As mentioned, sulphur poisoning may occur on the Pt surface, but we need to establish the effect  
425 of temperature and pressure on the surface behaviour. **Error! Reference source not found.** shows the  
426 phase diagram for S on the Pt (001), (011) and (111) surfaces. Overall, it can be seen that, compared to  
427 pressure, temperature has a bigger effect on the S surface coverage.

428 The adsorption of S onto the surfaces released energies of between 5 and 7 eV (Table 1). By adding the  
429 thermodynamic terms, it can be seen that the Pt surface is very susceptible to sulphur poisoning under  
430 experimental conditions, when the surface coverage will be  $\theta > 1$ . As the temperature increases,  
431 subsequent S atoms will react to form  $\text{S}_2$  and leave the surface, which is seen at  $\sim 700 - 900$  K on the  
432 (011) surface, although on the (001) and (111) surfaces, S or  $\text{S}_2$  only start to leave the surface at  $T >$   
433 1300 K. The temperature was only considered up to 2000 K, as Pt starts melting at 2047 K [84] beyond  
434 which it can no longer be considered a stable catalyst. The affinity of S adsorption to any Pt surface, even  
435 at very high temperatures, is a clear indication that where possible reactions should be designed to  
436 prohibit the formation of S as a by-product.

437 Figure 12 shows the phase diagram for SO on the Pt (001), (011) and (111) surfaces. The thermodynamic  
438 data show that for the adsorption of SO on both the (001) and (011) surfaces, coverages of  $\theta \geq 1$  can be  
439 expected. On the (001) surface, the coverage changes from  $\theta = 1.11$  to  $\theta = 1.00$  between 250 and 400  
440 K and even up to 1000 K, the (001) surface will be fully covered with SO. As such, changes in temperature  
441 and pressure cannot be utilised to clear the Pt surface of impurities. On the (011) surface, high coverages  
442 are sustained up to 350 and 800 K for the  $\text{SO}_{\text{Bridge}}$  and  $\text{SO}_{4\text{F}}$  configurations, respectively. At higher  
443 temperatures, some of the SO molecules will leave the surface without taking part in additional reactions,



444 but the surface is never entirely free from SO. Interestingly, on the (111) surface, the SO loading is lower,  
445 starting at  $\theta = 0.89$  and slowly decreasing to  $\theta = 0.44$  at  $T \geq 550$  K.

446 The thermodynamic influence on  $\text{SO}_3$  adsorption was also only considered up to 1000 K as shown in  
447 Figure 13. Similar to the trends with SO, it can be seen in the experimental range (200 -400 K), surface  
448 coverage is the highest on the (001) surface ( $\theta = 0.66$ ), followed by the (011) ( $0.44 < \theta < 0.56$ ) and (111)  
449 ( $\theta = 0.44$ ) surfaces. Here it can also be seen that temperature has a greater effect on surface coverage,  
450 compared to S and SO, possibly due to additional reactions taking place between subsequent  $\text{SO}_3$   
451 molecules. Two reactions that may occur include  $2 \text{SO}_3 \rightarrow \text{SO}$  and  $\text{SO}_4$  as was seen on the (011) surface,  
452 or  $2 \text{SO}_3 \rightarrow 2 \text{SO}_2 + \text{O}_2$ . The surface can be cleared of  $\text{SO}_3$  on both the (111) and (011) surfaces at  $T \geq$   
453 600 K and  $T \geq 800$  K, respectively.

454 During the investigation of  $\text{H}_2\text{O}$  and  $\text{SO}_2$  adsorption on the Pt surfaces [46–48], temperature played an  
455 important role on the surface coverage and that the surface can be cleared of both molecules at elevated  
456 temperatures. This is a clear indication that the HyS cycle is temperature sensitive and care should be  
457 taken during operation. Elevated temperatures cause firstly the  $\text{H}_2\text{O}$  molecules will desorb from the  
458 surface. This in turn could cause an increase in the  $\text{SO}_2$  concentration and lead to the formation of more  
459 by-products of  $\text{SO}_2$ , which in turn will impact the efficiency of the HyS cycle.

460

This is the author's peer reviewed, accepted manuscript. However, the online version of record will be different from this version once it has been copyedited and typeset.  
PLEASE CITE THIS ARTICLE AS DOI:10.1063/1.50043501

461

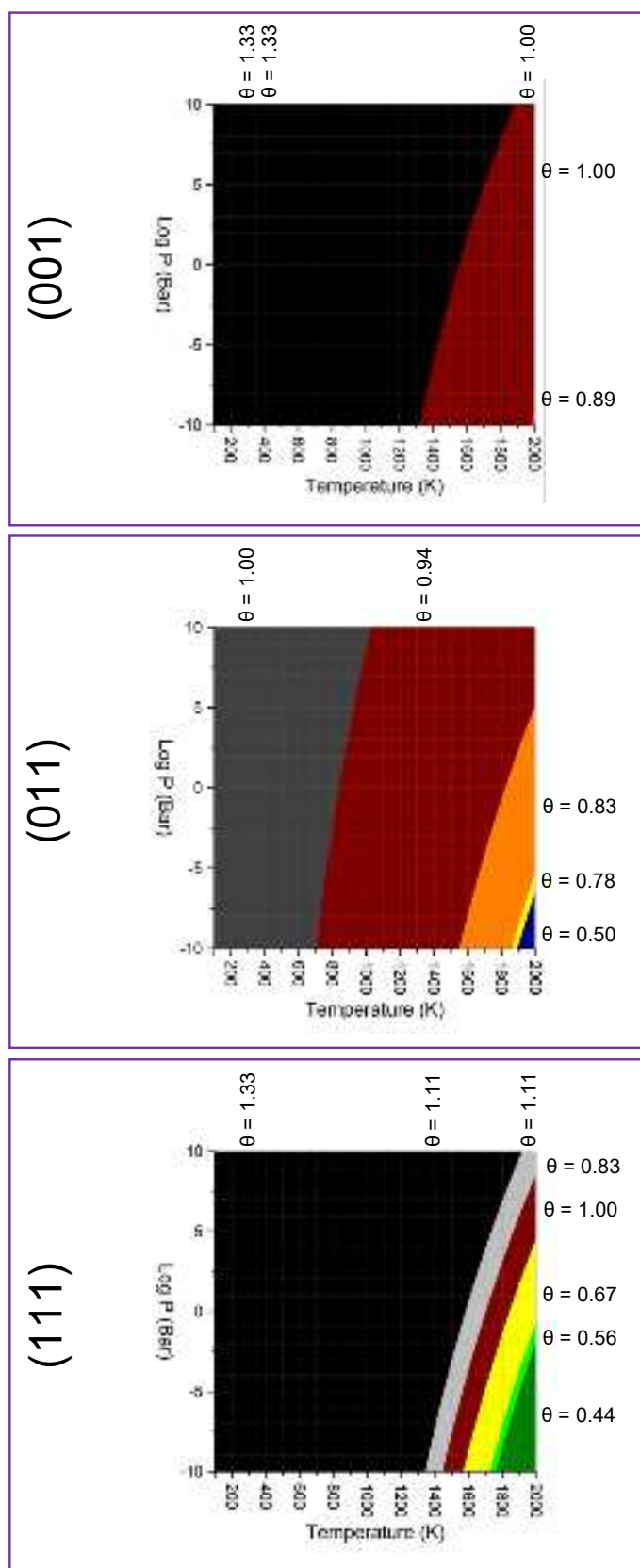
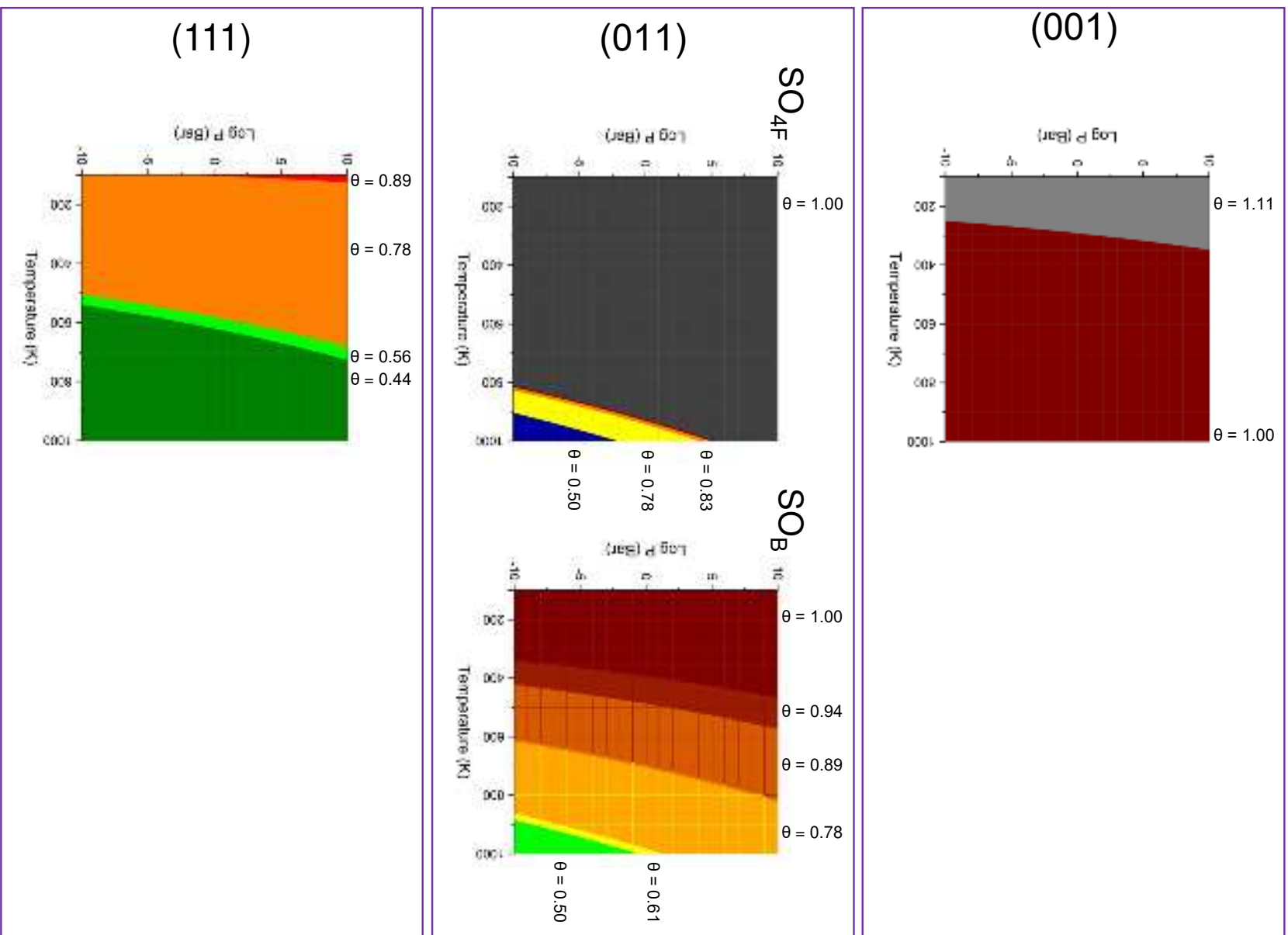
462  
463

Figure 11 – Surface phase diagrams in terms of pressure and temperature for the surface coverage of S on the Pt (001), (011) and (111) surfaces. Calculated surface coverage ( $\theta$ ) is given for each colour.

This is the author's peer reviewed, accepted manuscript. However, the online version of record will be different from this version once it has been copyedited and typeset.

PLEASE CITE THIS ARTICLE AS DOI:10.1063/5.0043501



464

465 Figure 12 – Surface phase diagrams in terms of pressure and temperature for the surface coverage of  
466 SO on the Pt (001), (011) and (111) surfaces. Calculated surface coverage ( $\theta$ ) is given for each colour.

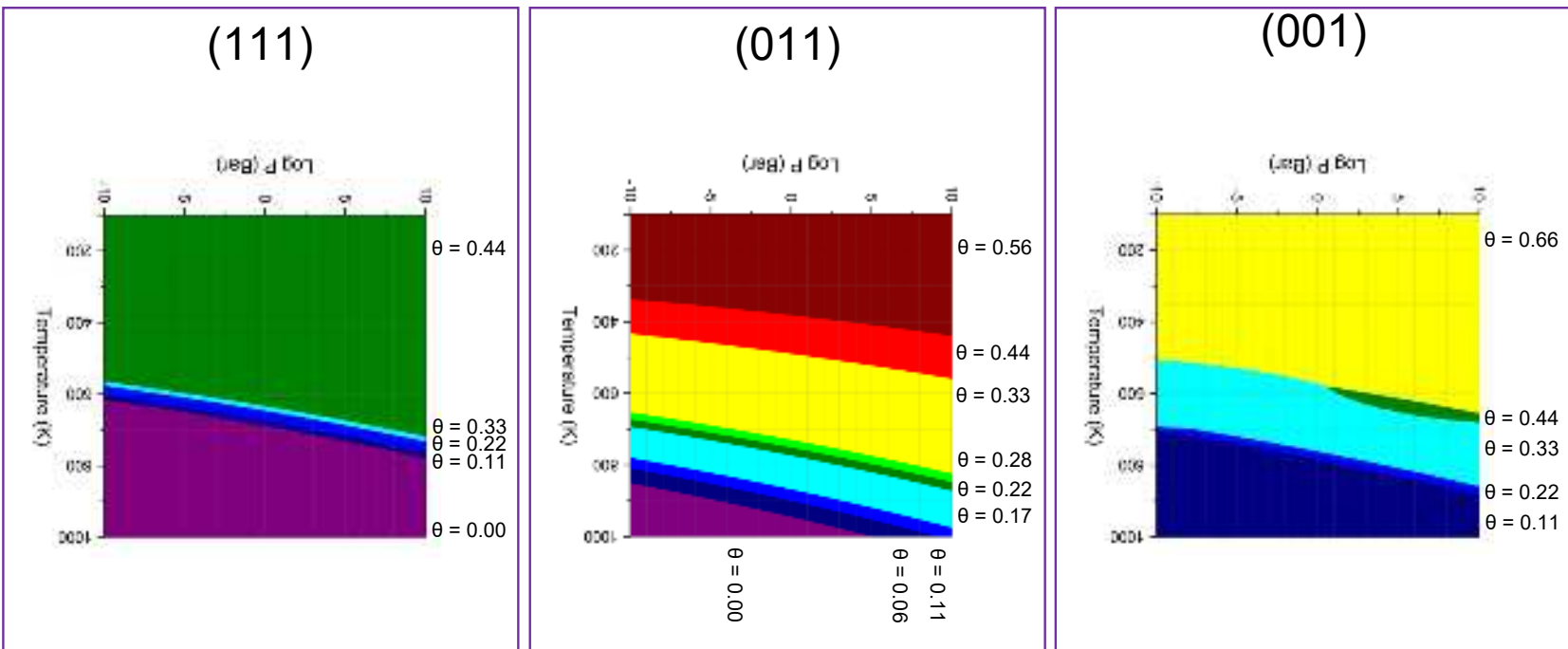
This is the author's peer reviewed, accepted manuscript. However, the online version of record will be different from this version once it has been copyedited and typeset.

PLEASE CITE THIS ARTICLE AS DOI:10.1063/5.0043501

467

468  
469

Figure 13 – Surface phase diagrams in terms of pressure and temperature for the surface coverage of  $\text{SO}_3$  on the Pt (001), (011) and (111) surfaces. Calculated surface coverage ( $\theta$ ) is given for each colour.



#### 470 4. Conclusions

471 Density functional theory calculations were employed to gain a detailed understanding of the behaviour  
472 of S, SO and SO<sub>3</sub> on the Pt (001), (011) and (111) surfaces. Adsorption of all three adsorbates as  
473 individual molecules was considered first on all the Pt surfaces. When elemental S was adsorbed, it  
474 preferred the 4F hollow site on both the (001) and (011) surfaces ( $E_{\text{ads}_001} = -7.09$  eV and  $E_{\text{ads}_011} = -5.47$   
475 eV, respectively) and the *fcc* hollow on the (111) surface ( $E_{\text{ads}_111} = -5.47$  eV). The adsorption of SO  
476 again showed a preference for the 4F hollow on the (001) surface ( $E_{\text{ads}_001} = -5.10$  eV), with two possible  
477 S,O-adsorptions in the bridge and 4F hollow sites on the (011) surface ( $E_{\text{ads}_011_{\text{bridge}}} = -3.56$  eV and  
478  $E_{\text{ads}_011_{4F}} = -3.57$  eV, respectively) and the *fcc* hollow on the (111) surface ( $E_{\text{ads}_111} = -5.47$  eV).  
479 Adsorption of SO<sub>3</sub> on the surface was preferred in a S,O,O bound configuration in the 4F ( $E_{\text{ads}_001} = -3.38$   
480 eV), 4F ( $E_{\text{ads}_011} = -2.68$  eV) and *fcc* ( $E_{\text{ads}_111} = -1.83$ eV) hollow adsorption sites on the (001), (011) and  
481 (111) surfaces, respectively. Overall, it was found that the higher the bond order, the more charge transfer  
482 occurs from the Pt surface to the adsorbate. In SO<sub>3</sub> in particular, we noted that the molecule configuration  
483 changed from planar to tetrahedral, a clear indication of chemisorption and activation of the molecule.

484 The surface coverage of all three molecules was increased on all the surfaces, until a monolayer was  
485 obtained. The highest surface coverage for S showed the trend  $(001)_S = (111)_S > (011)_S$ , for SO it was  
486  $(001)_{SO} > (011)_{SO} > (111)_{SO}$  and similar for SO<sub>3</sub>  $(001)_{SO_3} > (011)_{SO_3} > (111)_{SO_3}$ , which indicates that the  
487 (001) surface is more susceptible to catalyst poisoning by S species. It was also very evident that both  
488 the (001) and (111) surfaces were reactive towards S, leading to the formation of S<sub>2</sub>. We found no  
489 evidence of secondary reactions of SO on any for the Pt surfaces, but at high coverages of SO<sub>3</sub>, we noted  
490 the formation of SO<sub>2</sub> and SO<sub>4</sub>, especially on the (011) surface.

491 Thermodynamic effects were also investigated, where we have shown that pressure plays a minimal role  
492 in the surface coverage behaviour. An increase in the temperature up to 2000 K showed that the Pt  
493 surfaces would still be fully covered with S. The SO coverage showed  $\theta \geq 1.00$  on both the (001) and  
494 (011) surfaces, and  $\theta = 0.78$  on the (111) surface under the experimental temperature and pressure  
495 regime, in which the HyS cycle is operated. However, lower coverages of SO<sub>3</sub> were observed and the  
496 surface can be cleared at higher temperatures, i.e.  $T_{(001)} \geq 1000$  K,  $T_{(011)} \geq 800$  K and  $T_{(111)} \geq 600$  K.

497

#### 498 5. Acknowledgements

499 We acknowledge the Engineering and Physical Sciences Research Council (EPSRC grants No.  
500 EP/K016288/1 and EP/K009567/2) as well as the Economic and Social Research Council (ESRC grant  
501 No. ES/N013867/1) and the National Research Foundation of South Africa for funding under the Newton  
502 Programme and for a Post-Doctoral Fellowship (NRF grant no. 116728). This research was undertaken

503 using resources at North-West University, South Africa, and the Supercomputing Facilities at Cardiff  
504 University, UK, operated by ARCCA on behalf of Supercomputing Wales (SCW) projects, which is part-  
505 funded by the European Regional Development Fund (ERDF) via Welsh Government. We also  
506 acknowledge the use of facilities at the Centre for High-Performance Computing (CHPC), South Africa.

507

## 508 **6. Data Availability**

509 All data created during this research are openly available from Cardiff University's Research Portal: M.J.  
510 Ungerer, C.G.C.E. van Sittert and N.H. de Leeuw (2021). "Behaviour of S, SO and SO<sub>3</sub> on Pt (001), (011)  
511 and (111) surfaces: A DFT Study," Cardiff University's Research Portal, V. 1, Dataset.  
512 <http://doi.org/10.17035/d.2021.0126222709>.

513

## 514 **7. References**

- 515 [1] L. Newman, Atmospheric oxidation of sulfur dioxide: A review as viewed from power plant and  
516 smelter plume studies, *Atmos. Environ.* 15 (1981) 2231–2239. [https://doi.org/10.1016/0004-](https://doi.org/10.1016/0004-6981(81)90255-9)  
517 [6981\(81\)90255-9](https://doi.org/10.1016/0004-6981(81)90255-9).
- 518 [2] R.E. Huie, P. Neta, Chemical behavior of sulfur trioxide(1-) (SO<sub>3</sub>-) and sulfur pentoxide(1-) (SO<sub>5</sub>-  
519 ) radicals in aqueous solutions, *J. Phys. Chem.* 88 (1984) 5665–5669.  
520 <https://doi.org/10.1021/j150667a042>.
- 521 [3] Sulfur, in: *Chem. Elem.*, Elsevier, 1997: pp. 645–746. [https://doi.org/10.1016/B978-0-7506-3365-](https://doi.org/10.1016/B978-0-7506-3365-9.50021-3)  
522 [9.50021-3](https://doi.org/10.1016/B978-0-7506-3365-9.50021-3).
- 523 [4] Z. Klimont, S.J. Smith, J. Cofala, The last decade of global anthropogenic sulfur dioxide: 2000–  
524 2011 emissions, *Environ. Res. Lett.* 8 (2013) 014003. [https://doi.org/10.1088/1748-](https://doi.org/10.1088/1748-9326/8/1/014003)  
525 [9326/8/1/014003](https://doi.org/10.1088/1748-9326/8/1/014003).
- 526 [5] W. Aas, A. Mortier, V. Bowersox, R. Cherian, G. Faluvegi, H. Fagerli, J. Hand, Z. Klimont, C. Galy-  
527 Lacaux, C.M.B. Lehmann, C.L. Myhre, G. Myhre, D. Olivié, K. Sato, J. Quaas, P.S.P. Rao, M.  
528 Schulz, D. Shindell, R.B. Skeie, A. Stein, T. Takemura, S. Tsyro, R. Vet, X. Xu, Global and regional  
529 trends of atmospheric sulfur, *Sci. Rep.* 9 (2019) 953. [https://doi.org/10.1038/s41598-018-37304-](https://doi.org/10.1038/s41598-018-37304-0)  
530 [0](https://doi.org/10.1038/s41598-018-37304-0).
- 531 [6] Rt Hon Michael Gove, Clean Air Strategy Plan, 2019.  
532 [https://assets.publishing.service.gov.uk/government/uploads/system/uploads/attachment\\_data/fil](https://assets.publishing.service.gov.uk/government/uploads/system/uploads/attachment_data/file/770715/clean-air-strategy-2019.pdf)  
533 [e/770715/clean-air-strategy-2019.pdf](https://assets.publishing.service.gov.uk/government/uploads/system/uploads/attachment_data/file/770715/clean-air-strategy-2019.pdf).

- 534 [7] Q. Zhong, H. Shen, X. Yun, Y. Chen, Y. Ren, H. Xu, G. Shen, W. Du, J. Meng, W. Li, J. Ma, S.  
535 Tao, Global Sulfur Dioxide Emissions and the Driving Forces, *Environ. Sci. Technol.* 54 (2020)  
536 6508–6517. <https://doi.org/10.1021/acs.est.9b07696>.
- 537 [8] G.L. Smith, J.E. Eyley, X. Han, X. Zhang, J. Li, N.M. Jacques, H.G.W. Godfrey, S.P. Argent, L.J.  
538 McCormick McPherson, S.J. Teat, Y. Cheng, M.D. Frogley, G. Cinque, S.J. Day, C.C. Tang, T.L.  
539 Easun, S. Rudić, A.J. Ramirez-Cuesta, S. Yang, M. Schröder, Reversible coordinative binding and  
540 separation of sulfur dioxide in a robust metal–organic framework with open copper sites, *Nat.*  
541 *Mater.* 18 (2019) 1358–1365. <https://doi.org/10.1038/s41563-019-0495-0>.
- 542 [9] S. Díaz-Abad, M. Millán, M.A. Rodrigo, J. Lobato, Review of Anodic Catalysts for SO<sub>2</sub> Depolarized  
543 Electrolysis for “Green Hydrogen” Production, *Catalysts.* 9 (2019) 63.  
544 <https://doi.org/10.3390/catal9010063>.
- 545 [10] D.R. Uzun, E. Razkazova-Velkova, V. Beschkov, K. Petrov, A Method for the Simultaneous  
546 Cleansing of H<sub>2</sub>S and SO<sub>2</sub>, *Int. J. Electrochem.* 2016 (2016) 1–5.  
547 <https://doi.org/10.1155/2016/7628761>.
- 548 [11] C.-C. Cormos, Hydrogen production from fossil fuels with carbon capture and storage based on  
549 chemical looping systems, *Int. J. Hydrogen Energy.* 36 (2011) 5960–5971.  
550 <https://doi.org/10.1016/j.ijhydene.2011.01.170>.
- 551 [12] M. Ni, D.Y.C. Leung, M.K.H. Leung, K. Sumathy, An overview of hydrogen production from  
552 biomass, *Fuel Process. Technol.* 87 (2006) 461–472.  
553 <https://doi.org/10.1016/j.fuproc.2005.11.003>.
- 554 [13] C. Acar, I. Dincer, G.F. Naterer, Review of photocatalytic water-splitting methods for sustainable  
555 hydrogen production, *Int. J. Energy Res.* 40 (2016) 1449–1473. <https://doi.org/10.1002/er.3549>.
- 556 [14] A. Ursúa, L.M. Gandía, P. Sanchis, Hydrogen Production From Water Electrolysis: Current Status  
557 and Future Trends, *Proc. IEEE.* 100 (2012) 410–426.  
558 <https://doi.org/10.1109/JPROC.2011.2156750>.
- 559 [15] F. de Bruijn, The current status of fuel cell technology for mobile and stationary applications, *Green*  
560 *Chem.* 7 (2005) 132–150. <https://doi.org/10.1039/b415317k>.
- 561 [16] L. Baharudin, M. James Watson, Hydrogen applications and research activities in its production  
562 routes through catalytic hydrocarbon conversion, *Rev. Chem. Eng.* 34 (2017).  
563 <https://doi.org/10.1515/revce-2016-0040>.
- 564 [17] L. Schlapbach, A. Züttel, Hydrogen-storage materials for mobile applications, in: *Mater. Sustain.*

- 565 Energy, Co-Published with Macmillan Publishers Ltd, UK, 2010: pp. 265–270.  
566 [https://doi.org/10.1142/9789814317665\\_0038](https://doi.org/10.1142/9789814317665_0038).
- 567 [18] X. Lin, K.C. Hass, W.F. Schneider, B.L. Trout, Chemistry of Sulfur Oxides on Transition Metals I:  
568 Configurations, Energetics, Orbital Analyses, and Surface Coverage Effects of SO<sub>2</sub> on Pt(111),  
569 J. Phys. Chem. B. 106 (2002) 12575–12583. <https://doi.org/10.1021/jp026128f>.
- 570 [19] X. Lin, W.F. Schneider, B.L. Trout, Chemistry of sulfur oxides on transition metals. II.  
571 Thermodynamics of sulfur oxides on platinum(111), J. Phys. Chem. B. 108 (2004) 250–264.  
572 <https://doi.org/10.1021/jp035306h>.
- 573 [20] X. Lin, W.F. Schneider, B.L. Trout, Chemistry of sulfur oxides on transition metals. III. Oxidation of  
574 SO<sub>2</sub> and self-diffusion of O, SO<sub>2</sub>, and SO<sub>3</sub> on Pt(111), J. Phys. Chem. B. 108 (2004) 13329–  
575 13340. <https://doi.org/10.1021/jp048507>.
- 576 [21] J.A. O'Brien, J.T. Hinkley, S.W. Donne, S.E. Lindquist, The electrochemical oxidation of aqueous  
577 sulfur dioxide: A critical review of work with respect to the hybrid sulfur cycle, Electrochim. Acta.  
578 55 (2010) 573–591. <https://doi.org/10.1016/j.electacta.2009.09.067>.
- 579 [22] M. Polcik, L. Wilde, J. Haase, B. Brena, D. Cocco, G. Comelli, G. Paolucci, Adsorption and  
580 temperature-dependent decomposition of SO<sub>2</sub> on Cu(100) and Cu(111): A fast and high-resolution  
581 core-level spectroscopy study, Phys. Rev. B. 53 (1996) 13720–13724.  
582 <https://doi.org/10.1103/PhysRevB.53.13720>.
- 583 [23] M. Polčik, L. Wilde, J. Haase, SO<sub>2</sub>-induced surface reconstruction of Cu(111): An x-ray-absorption  
584 fine-structure study, Phys. Rev. B. 57 (1998) 1868–1874.  
585 <https://doi.org/10.1103/PhysRevB.57.1868>.
- 586 [24] M.S. Wilburn, W.S. Epling, SO<sub>2</sub> adsorption and desorption characteristics of Pd and Pt catalysts:  
587 Precious metal crystallite size dependence, Appl. Catal. A Gen. 534 (2017) 85–93.  
588 <https://doi.org/10.1016/j.apcata.2017.01.015>.
- 589 [25] J.A. Rodriguez, J.M. Ricart, A. Clotet, F. Illas, Density functional studies on the adsorption and  
590 decomposition of SO<sub>2</sub> on Cu(100), J. Chem. Phys. 115 (2001) 454–465.  
591 <https://doi.org/10.1063/1.1377884>.
- 592 [26] T. Yokoyama, S. Terada, S. Yagi, A. Imanishi, S. Takenaka, Y. Kitajima, T. Ohta, Surface  
593 structures and electronic properties of SO<sub>2</sub> adsorbed on Ni(111) and Ni(100) studied by S K-edge  
594 X-ray absorption fine structure spectroscopy, Surf. Sci. 324 (1995) 25–34.  
595 [https://doi.org/10.1016/0039-6028\(94\)00692-X](https://doi.org/10.1016/0039-6028(94)00692-X).



- 596 [27] S. Terada, A. Imanishi, T. Yokoyama, S. Takenaka, Y. Kitajima, T. Ohta, Surface structure of SO<sub>2</sub>  
597 adsorbed on Ni(110) studied by S K-edge X-ray absorption fine structure spectroscopy, *Surf. Sci.*  
598 336 (1995) 55–62. [https://doi.org/10.1016/0039-6028\(95\)00514-5](https://doi.org/10.1016/0039-6028(95)00514-5).
- 599 [28] P. Zebisch, M. Weinelt, H.-P. Steinrück, Sulphur dioxide adsorption on the Ni(110) surface, *Surf.*  
600 *Sci.* 295 (1993) 295–305. [https://doi.org/10.1016/0039-6028\(93\)90276-P](https://doi.org/10.1016/0039-6028(93)90276-P).
- 601 [29] J. Ahner, A. Effendy, K. Vajen, H.-W. Wassmuth, Chemisorption and multilayer adsorption of SO<sub>2</sub>  
602 on Ag(111) and Ag(110), *Vacuum.* 41 (1990) 98–101. [https://doi.org/10.1016/0042-](https://doi.org/10.1016/0042-207X(90)90285-7)  
603 [207X\(90\)90285-7](https://doi.org/10.1016/0042-207X(90)90285-7).
- 604 [30] J.L. Solomon, R.J. Madix, W. Wurth, J. Stohr, NEXAFS and EELS study of the orientation of sulfur  
605 dioxide on silver(110), *J. Phys. Chem.* 95 (1991) 3687–3691. <https://doi.org/10.1021/j100162a046>.
- 606 [31] R.C. Ku, P. Wynblatt, SO<sub>2</sub> adsorption on Rh(110) and Pt(110) surfaces, *Appl. Surf. Sci.* 8 (1981)  
607 250–259. [https://doi.org/10.1016/0378-5963\(81\)90120-3](https://doi.org/10.1016/0378-5963(81)90120-3).
- 608 [32] J.A. Rodriguez, T. Jirsak, S. Chaturvedi, Reaction of S<sub>2</sub> and SO<sub>2</sub> with Pd/Rh(111) surfaces:  
609 Effects of metal–metal bonding on sulfur poisoning, *J. Chem. Phys.* 110 (1999) 3138–3147.  
610 <https://doi.org/10.1063/1.477910>.
- 611 [33] S. Terada, M. Sakano, Y. Kitajima, T. Yokoyama, T. Ohta, Adsorption of SO<sub>2</sub> on Pd(100) Studied  
612 by S K-Edge XAFS, *Le J. Phys. IV.* 7 (1997) C2-703-C2-704. <https://doi.org/10.1051/jp4:1997211>.
- 613 [34] M.L. Burke, R.J. Madix, Hydrogen on Pd(100)-S: the effect of sulfur on precursor mediated  
614 adsorption and desorption, *Surf. Sci.* 237 (1990) 1–19. [https://doi.org/10.1016/0039-](https://doi.org/10.1016/0039-6028(90)90515-A)  
615 [6028\(90\)90515-A](https://doi.org/10.1016/0039-6028(90)90515-A).
- 616 [35] J.M. Saleh, Interaction of sulphur compounds with palladium, *Trans. Faraday Soc.* 66 (1970) 242.  
617 <https://doi.org/10.1039/tf9706600242>.
- 618 [36] M.L. Burke, R.J. Madix, SO<sub>2</sub> structure and reactivity on clean and sulfur modified Pd(100), *Surf.*  
619 *Sci.* 194 (1988) 223–244. [https://doi.org/10.1016/0039-6028\(94\)91257-2](https://doi.org/10.1016/0039-6028(94)91257-2).
- 620 [37] S. Astegger, E. Bechtold, Adsorption of sulfur dioxide and the interaction of coadsorbed oxygen  
621 and sulfur on Pt(111), *Surf. Sci.* 122 (1982) 491–504. [https://doi.org/10.1016/0039-](https://doi.org/10.1016/0039-6028(82)90098-X)  
622 [6028\(82\)90098-X](https://doi.org/10.1016/0039-6028(82)90098-X).
- 623 [38] U. Köhler, H.-W. Wassmuth, SO<sub>2</sub> adsorption and desorption kinetics on Pt(111), *Surf. Sci.* 126  
624 (1983) 448–454. [https://doi.org/10.1016/0039-6028\(83\)90742-2](https://doi.org/10.1016/0039-6028(83)90742-2).
- 625 [39] Y.-M. Sun, D. Sloan, D.J. Alberas, M. Kovar, Z.-J. Sun, J.M. White, SO<sub>2</sub> adsorption on Pt(111):

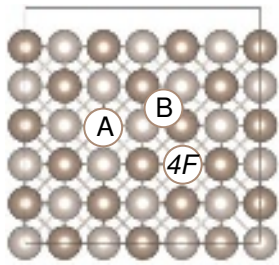
- 626 HREELS, XPS and UPS study, *Surf. Sci.* 319 (1994) 34–44. <https://doi.org/10.1016/0039->  
627 6028(94)90567-3.
- 628 [40] M. Polčik, L. Wilde, J. Haase, B. Brena, G. Comelli, G. Paolucci, High-resolution XPS and NEXAFS  
629 study of SO<sub>2</sub> adsorption on Pt(111): two surface SO<sub>2</sub> species, *Surf. Sci.* 381 (1997) L568–L572.  
630 [https://doi.org/10.1016/S0039-6028\(97\)00060-5](https://doi.org/10.1016/S0039-6028(97)00060-5).
- 631 [41] H.R. Colón-Mercado, D.T. Hobbs, Catalyst evaluation for a sulfur dioxide-depolarized electrolyzer,  
632 *Electrochem. Commun.* 9 (2007) 2649–2653. <https://doi.org/10.1016/j.elecom.2007.08.015>.
- 633 [42] P.W.T. Lu, R.L. Ammon, An Investigation of Electrode Materials for the Anodic Oxidation of Sulfur  
634 Dioxide in Concentrated Sulfuric Acid, *J. Electrochem. Soc.* 127 (1980) 2610.  
635 <https://doi.org/10.1149/1.2129530>.
- 636 [43] A.J. Appleby, B. Pinchon, Electrochemical aspects of the H<sub>2</sub>SO<sub>4</sub>SO<sub>2</sub> thermoelectrochemical cycle  
637 for hydrogen production, *Int. J. Hydrogen Energy.* 5 (1980) 253–267. <https://doi.org/10.1016/0360->  
638 3199(80)90070-1.
- 639 [44] B. Meyer, Elemental sulfur, *Chem. Rev.* 76 (1976) 367–388. <https://doi.org/10.1021/cr60301a003>.
- 640 [45] B.D. Struck, R. Junginger, D. Boltersdorf, J. Gehrman, The anodic oxidation of sulfur dioxide in  
641 the sulfuric acid hybrid cycle, *Int. J. Hydrogen Energy.* 5 (1980) 487–497.  
642 [https://doi.org/10.1016/0360-3199\(80\)90055-5](https://doi.org/10.1016/0360-3199(80)90055-5).
- 643 [46] M.J. Ungerer, D. Santos-Carballal, A. Cadi-Essadek, C.G.C.E. van Sittert, N.H. de Leeuw,  
644 Interaction of H<sub>2</sub>O with the Platinum Pt (001), (011) and (111) Surfaces: A Density Functional  
645 Theory Study with Long-Range Dispersion Corrections, *J. Phys. Chem. C.* (2019)  
646 [acs.jpcc.9b06136](https://doi.org/10.1021/acs.jpcc.9b06136). <https://doi.org/10.1021/acs.jpcc.9b06136>.
- 647 [47] M.J. Ungerer, D. Santos-Carballal, A. Cadi-Essadek, C.G.C.E. Van Sittert, N.H. de Leeuw,  
648 Interaction of SO<sub>2</sub> with the Platinum (001), (011) and (111) Surfaces: A DFT Study, *Surf. Chem.*  
649 *Catal.* (2020). [https://www.mdpi.com/journal/catalysts/special\\_issues/surf\\_catal](https://www.mdpi.com/journal/catalysts/special_issues/surf_catal).
- 650 [48] M.J. Ungerer, D. Santos-Carballal, C.G.C.E. van Sittert, N.H. De Leeuw, Competitive Adsorption  
651 of H<sub>2</sub>O and SO<sub>2</sub> on Catalytic Platinum Surfaces: a Density Functional Theory Study, *South African*  
652 *Chem. Inst. SPECIAL ED* (2020). <https://doi.org/10.17159/0379-4350/2020/v74a00>.
- 653 [49] G. Kresse, J. Hafner, Ab initio molecular dynamics for liquid metals, *Phys. Rev. B.* 47 (1993) 558–  
654 561. <https://doi.org/10.1103/PhysRevB.47.558>.
- 655 [50] G. Kresse, J. Hafner, Ab initio molecular-dynamics simulation of the liquid-metalamorphous-  
656 semiconductor transition in germanium, *Phys. Rev. B.* 49 (1994) 14251–14269.

- 657 <https://doi.org/10.1103/PhysRevB.49.14251>.
- 658 [51] G. Kresse, J. Furthmüller, Efficient iterative schemes for ab initio total-energy calculations using a  
659 plane-wave basis set, *Phys. Rev. B.* 54 (1996) 11169–11186.  
660 <https://doi.org/10.1103/PhysRevB.54.11169>.
- 661 [52] G. Kresse, J. Furthmüller, Efficiency of ab-initio total energy calculations for metals and  
662 semiconductors using a plane-wave basis set, *Comput. Mater. Sci.* 6 (1996) 15–50.  
663 [https://doi.org/10.1016/0927-0256\(96\)00008-0](https://doi.org/10.1016/0927-0256(96)00008-0).
- 664 [53] P.E. Blöchl, Projector augmented-wave method, *Phys. Rev. B.* 50 (1994) 17953–17979.  
665 <https://doi.org/10.1103/PhysRevB.50.17953>.
- 666 [54] G. Kresse, D. Joubert, From ultrasoft pseudopotentials to the projector augmented-wave method,  
667 *Phys. Rev. B.* 59 (1999) 1758–1775. <https://doi.org/10.1103/PhysRevB.59.1758>.
- 668 [55] J.P. Perdew, K. Burke, M. Ernzerhof, Generalized Gradient Approximation Made Simple, *Phys.*  
669 *Rev. Lett.* 77 (1996) 3865–3868. <https://doi.org/10.1103/PhysRevLett.77.3865>.
- 670 [56] S. Grimme, S. Ehrlich, L. Goerigk, Effect of the damping function in dispersion corrected density  
671 functional theory, *J. Comput. Chem.* 32 (2011) 1456–1465. <https://doi.org/10.1002/jcc.21759>.
- 672 [57] S. Posada-Pérez, D. Santos-Carballal, U. Terranova, A. Roldan, F. Illas, N.H. de Leeuw, CO<sub>2</sub>  
673 interaction with violarite (FeNi<sub>2</sub>S<sub>4</sub>) surfaces: a dispersion-corrected DFT study, *Phys. Chem.*  
674 *Chem. Phys.* 20 (2018) 20439–20446. <https://doi.org/10.1039/C8CP03430C>.
- 675 [58] S.S. Tafreshi, A. Roldan, N.Y. Dzade, N.H. de Leeuw, Adsorption of hydrazine on the perfect and  
676 defective copper (111) surface: A dispersion-corrected DFT study, *Surf. Sci.* 622 (2014) 1–8.  
677 <https://doi.org/10.1016/j.susc.2013.11.013>.
- 678 [59] N.Y. Dzade, A. Roldan, N.H. de Leeuw, Activation and dissociation of CO<sub>2</sub> on the (001), (011),  
679 and (111) surfaces of mackinawite (FeS): A dispersion-corrected DFT study, *J. Chem. Phys.* 143  
680 (2015) 094703. <https://doi.org/10.1063/1.4929470>.
- 681 [60] A.K. Mishra, A. Roldan, N.H. de Leeuw, CuO Surfaces and CO<sub>2</sub> Activation: A Dispersion-  
682 Corrected DFT+ U Study, *J. Phys. Chem. C.* 120 (2016) 2198–2214.  
683 <https://doi.org/10.1021/acs.jpcc.5b10431>.
- 684 [61] S. Grimme, J. Antony, S. Ehrlich, H. Krieg, A consistent and accurate ab initio parametrization of  
685 density functional dispersion correction (DFT-D) for the 94 elements H-Pu, *J. Chem. Phys.* 132  
686 (2010) 154104. <https://doi.org/10.1063/1.3382344>.

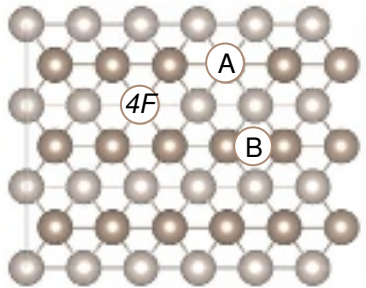
- 687 [62] M. Methfessel, A.T. Paxton, High-precision sampling for Brillouin-zone integration in metals, *Phys.*  
688 *Rev. B.* 40 (1989) 3616–3621. <https://doi.org/10.1103/PhysRevB.40.3616>.
- 689 [63] P.E. Blöchl, O. Jepsen, O.K. Andersen, Improved tetrahedron method for Brillouin-zone  
690 integrations, *Phys. Rev. B.* 49 (1994) 16223–16233. <https://doi.org/10.1103/PhysRevB.49.16223>.
- 691 [64] G. Corbel, M. Topić, A. Gibaud, C.I. Lang, Selective dry oxidation of the ordered Pt-11.1 at.% v  
692 alloy surface evidenced by in situ temperature-controlled X-ray diffraction, *J. Alloys Compd.* 509  
693 (2011) 6532–6538. <https://doi.org/10.1016/j.jallcom.2011.03.079>.
- 694 [65] H.J. Monkhorst, J.D. Pack, Special points for Brillouin-zon integrations, *Phys. Rev. B.* 13 (1976)  
695 5188–5192. <https://doi.org/10.1103/PhysRevB.16.1748>.
- 696 [66] J.W. Arblaster, Crystallographic properties of platinum, *Platin. Met. Rev.* 41 (1997) 12–21.  
697 <https://doi.org/http://www.technology.matthey.com/article/41/1/12-21/>.
- 698 [67] J.W. Arblaster, Crystallographic properties of platinum (Errata), *Platin. Met. Rev.* 50 (2006) 118–  
699 119. <https://doi.org/10.1595/147106706X129088>.
- 700 [68] G.W. Watson, E.T. Kelsey, N.H. de Leeuw, D.J. Harris, S.C. Parker, Atomistic simulation of  
701 dislocations, surfaces and interfaces in MgO, *J. Chem. Soc. Faraday Trans.* 92 (1996) 433.  
702 <https://doi.org/10.1039/ft9969200433>.
- 703 [69] G. Henkelman, A. Arnaldsson, H. Jónsson, A fast and robust algorithm for Bader decomposition  
704 of charge density, *Comput. Mater. Sci.* 36 (2006) 354–360.  
705 <https://doi.org/10.1016/j.commatsci.2005.04.010>.
- 706 [70] E. Sanville, S.D. Kenny, R. Smith, G. Henkelman, Improved grid-based algorithm for Bader charge  
707 allocation, *J. Comput. Chem.* 28 (2007) 899–908. <https://doi.org/10.1002/jcc.20575>.
- 708 [71] W. Tang, E. Sanville, G. Henkelman, A grid-based Bader analysis algorithm without lattice bias.,  
709 *J. Phys. Condens. Matter.* 21 (2009) 084204. <https://doi.org/10.1088/0953-8984/21/8/084204>.
- 710 [72] M. Yu, D.R. Trinkle, Accurate and efficient algorithm for Bader charge integration, *J. Chem. Phys.*  
711 134 (2011) 1–8. <https://doi.org/10.1063/1.3553716>.
- 712 [73] S.S. Tafreshi, A. Roldan, N.H. de Leeuw, Hydrazine network on Cu(111) surface: A Density  
713 Functional Theory approach, *Surf. Sci.* 637–638 (2015) 140–148.  
714 <https://doi.org/10.1016/j.susc.2015.04.001>.
- 715 [74] D. Santos-Carballal, A. Roldan, R. Grau-Crespo, N.H. de Leeuw, A DFT study of the structures,  
716 stabilities and redox behaviour of the major surfaces of magnetite Fe<sub>3</sub>O<sub>4</sub>, *Phys. Chem. Chem.*

- 717 Phys. 16 (2014) 21082–21097. <https://doi.org/10.1039/C4CP00529E>.
- 718 [75] M. Chase, NIST-JANAF Thermochemical Tables, 4th Edition, 1998. [https://doi.org/citeulike-article-](https://doi.org/citeulike-article-id:12140840)  
719 [id:12140840](https://doi.org/citeulike-article-id:12140840).
- 720 [76] J.-H. Wang, M. Liu, Computational study of sulfur–nickel interactions: A new S–Ni phase diagram,  
721 Electrochem. Commun. 9 (2007) 2212–2217. <https://doi.org/10.1016/j.elecom.2007.06.022>.
- 722 [77] W.R. Tyson, W.A. Miller, Surface free energies of solid metals: Estimation from liquid surface  
723 tension measurements, Surf. Sci. 62 (1977) 267–276. [https://doi.org/10.1016/0039-](https://doi.org/10.1016/0039-6028(77)90442-3)  
724 [6028\(77\)90442-3](https://doi.org/10.1016/0039-6028(77)90442-3).
- 725 [78] Z. Jian-Min, M. Fei, X. Ke-Wei, Calculation of the surface energy of fcc metals with modified  
726 embedded-atom method, Chinese Phys. 13 (2004) 1082–1090. [https://doi.org/10.1088/1009-](https://doi.org/10.1088/1009-1963/13/7/020)  
727 [1963/13/7/020](https://doi.org/10.1088/1009-1963/13/7/020).
- 728 [79] D.R. Alfonso, Computational Studies of Experimentally Observed Structures of Sulfur on Metal  
729 Surfaces, J. Phys. Chem. C. 115 (2011) 17077–17091. <https://doi.org/10.1021/jp2048426>.
- 730 [80] C.R. Bernard Rodríguez, J.A. Santana, Adsorption and diffusion of sulfur on the (111), (100), (110),  
731 and (211) surfaces of FCC metals: Density functional theory calculations, J. Chem. Phys. 149  
732 (2018) 204701. <https://doi.org/10.1063/1.5063464>.
- 733 [81] B.A. Lindquist, T.H. Dunning, The nature of the SO bond of chlorinated sulfur–oxygen compounds,  
734 Theor. Chem. Acc. 133 (2014) 1443. <https://doi.org/10.1007/s00214-013-1443-8>.
- 735 [82] R.J. Gillespie, E.A. Robinson, the Sulphur–Oxygen Bond in Sulphuryl and Thionyl Compounds:  
736 Correlation of Stretching Frequencies and Force Constants With Bond Lengths, Bond Angles, and  
737 Bond Orders, Can. J. Chem. 41 (1963) 2074–2085. <https://doi.org/10.1139/v63-299>.
- 738 [83] G. Dai, X. Wang, H. You, Y. Wang, Z. Shan, H. Tan, Catalytic function of ferric oxide and effect of  
739 water on the formation of sulfur trioxide, J. Environ. Manage. 264 (2020) 110499.  
740 <https://doi.org/10.1016/j.jenvman.2020.110499>.
- 741 [84] G.A. Slack, Platinum as a Thermal Conductivity Standard, J. Appl. Phys. 35 (1964) 339–344.  
742 <https://doi.org/10.1063/1.1713313>.
- 743

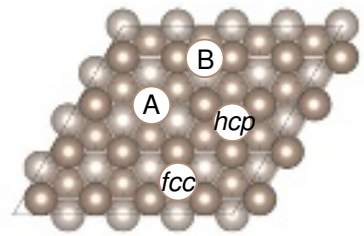
(001)



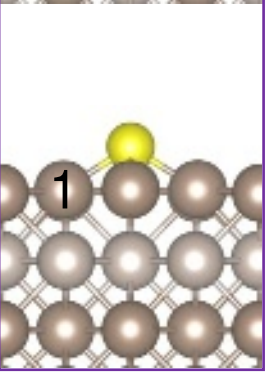
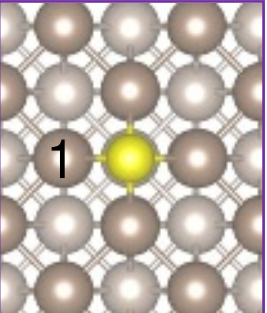
(011)



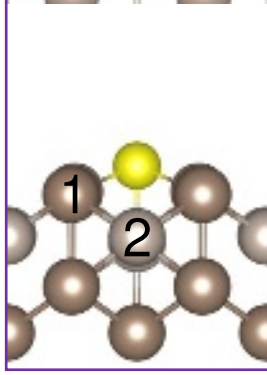
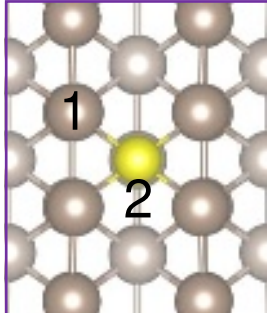
(111)



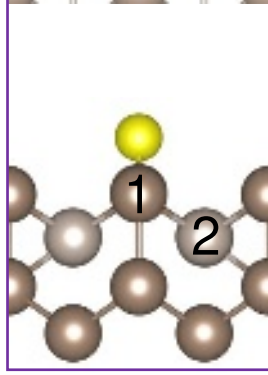
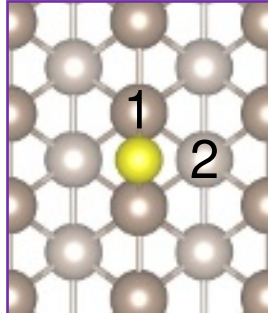
$(001)_{4F}$



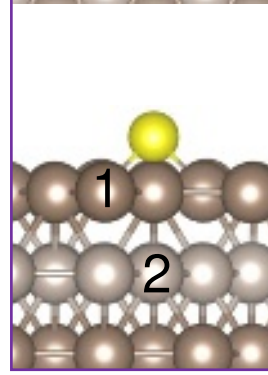
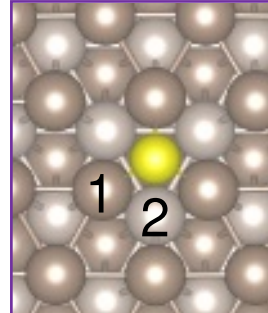
$(011)_{4F}$



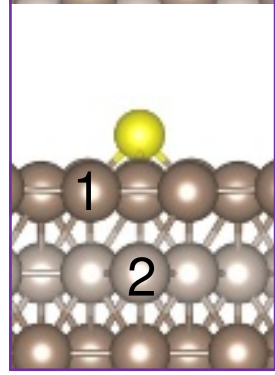
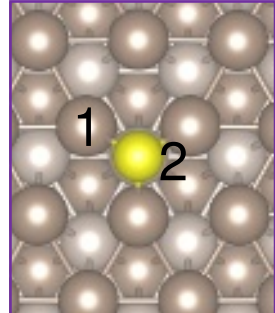
$(011)_B$



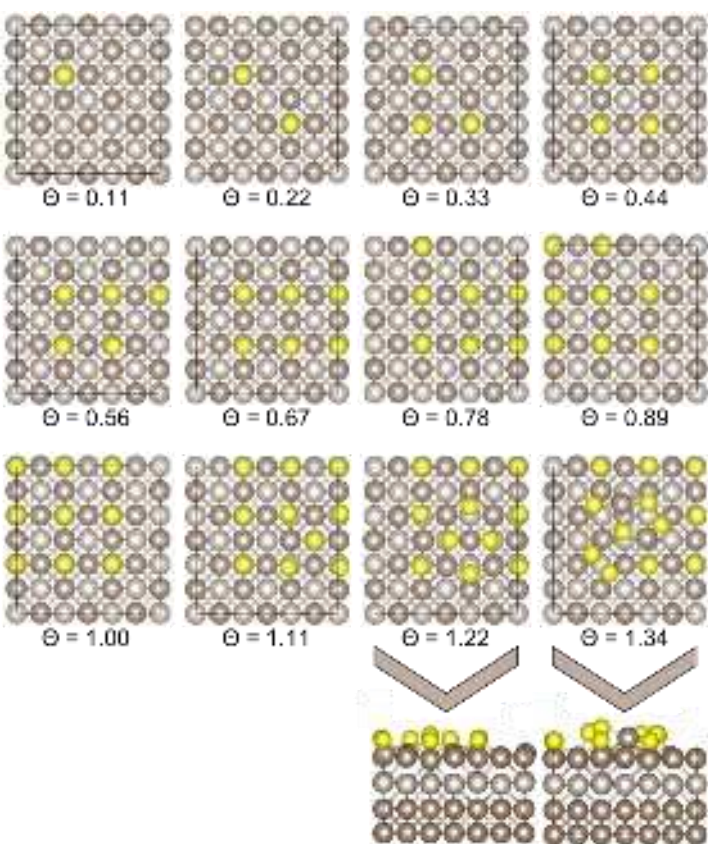
$(111)_{fcc}$



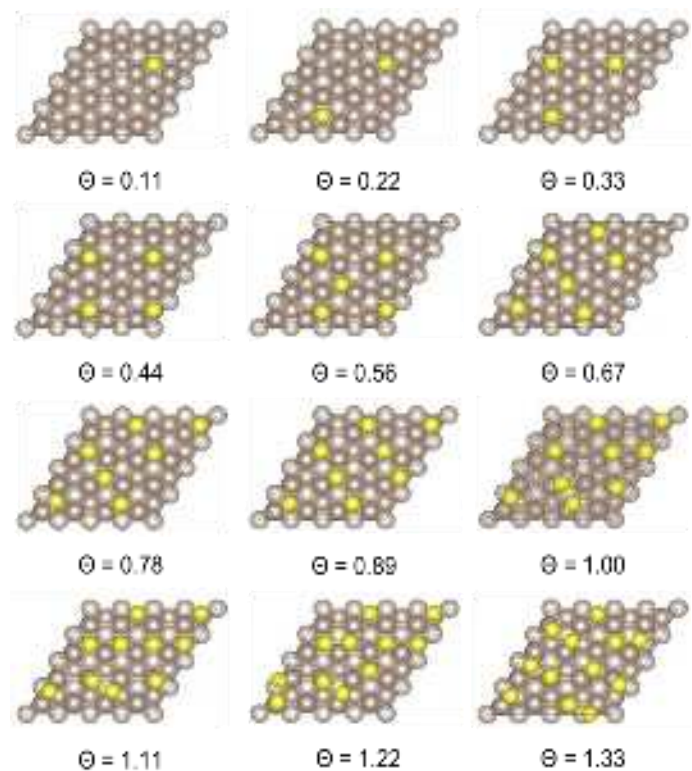
$(111)_{hcp}$



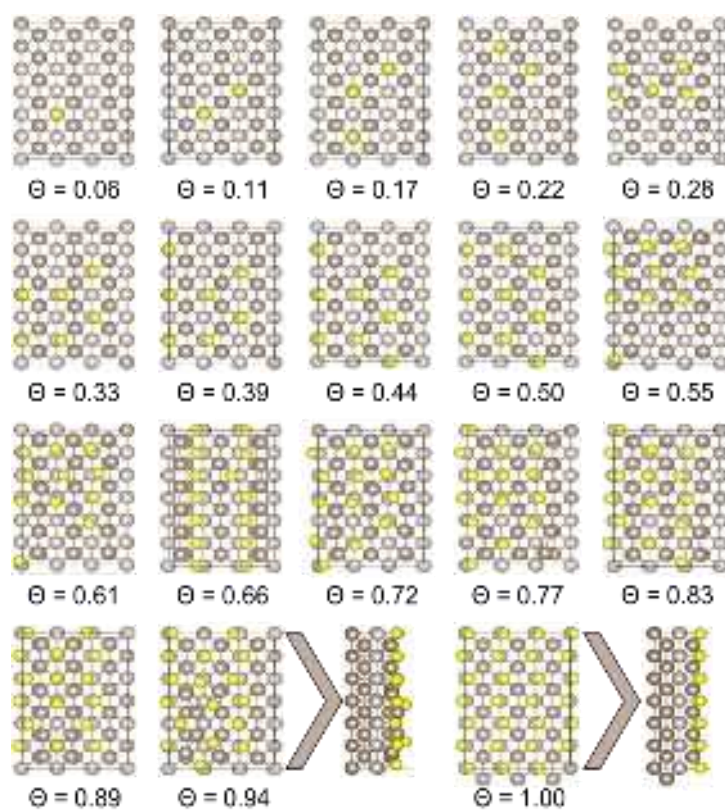
Pt (001)



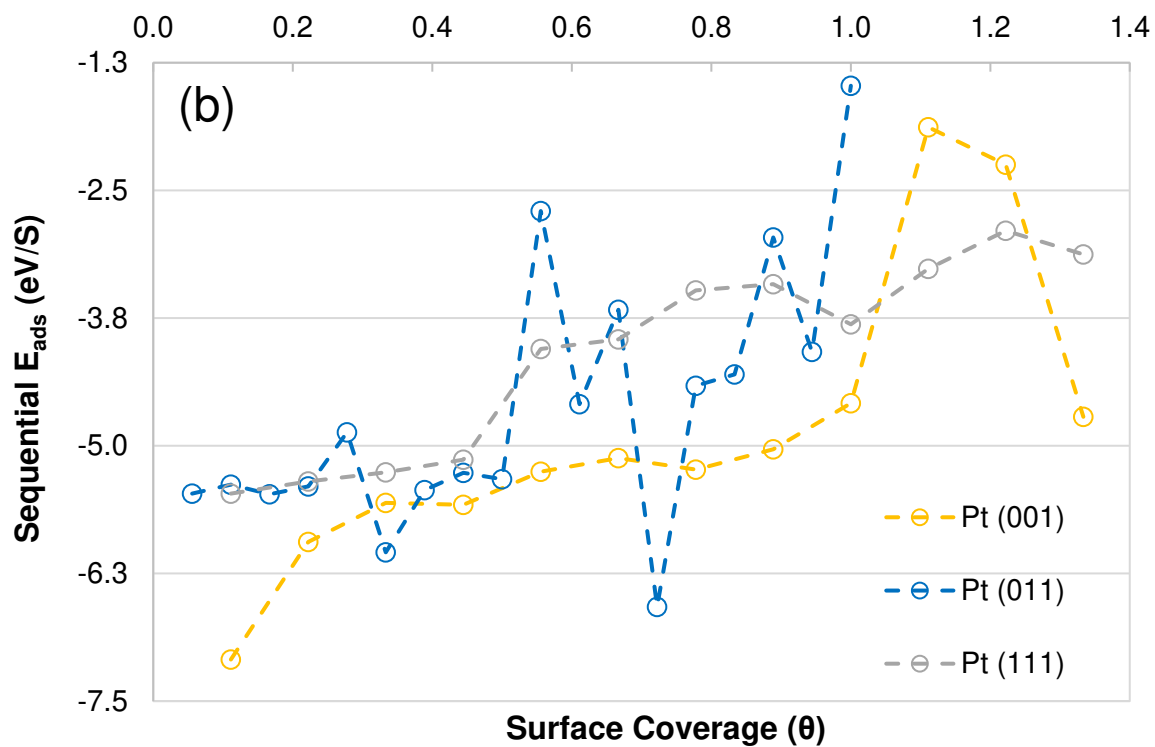
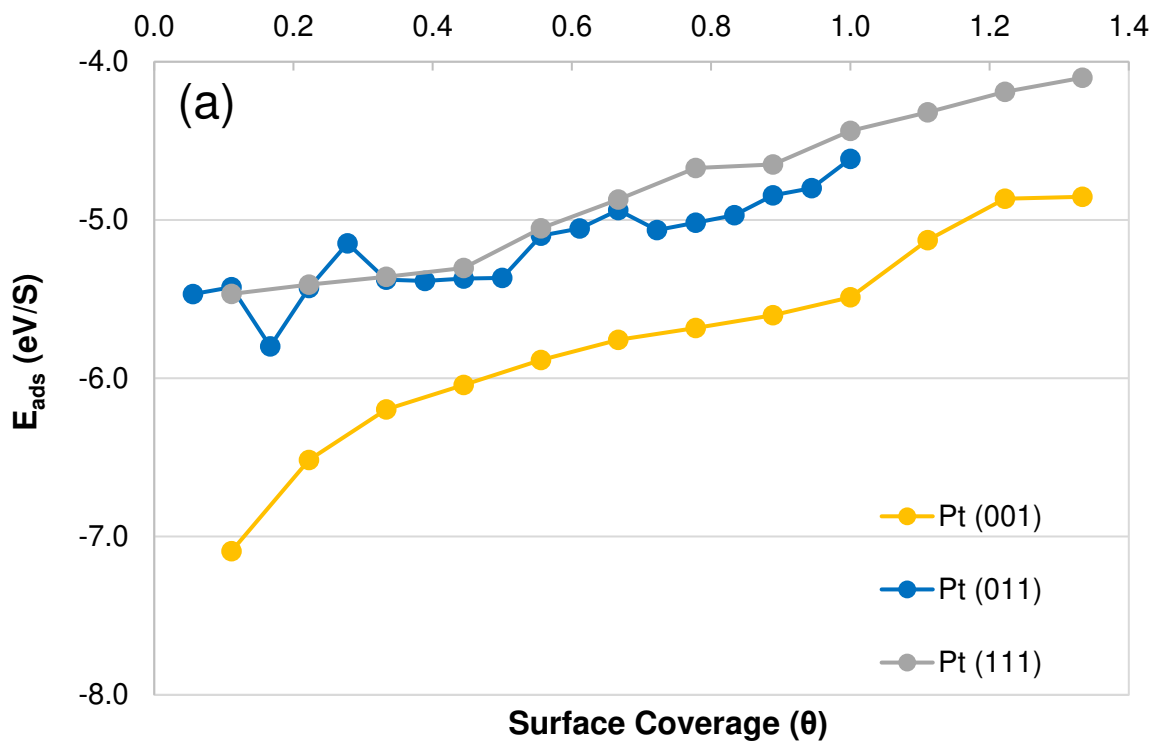
Pt (111)

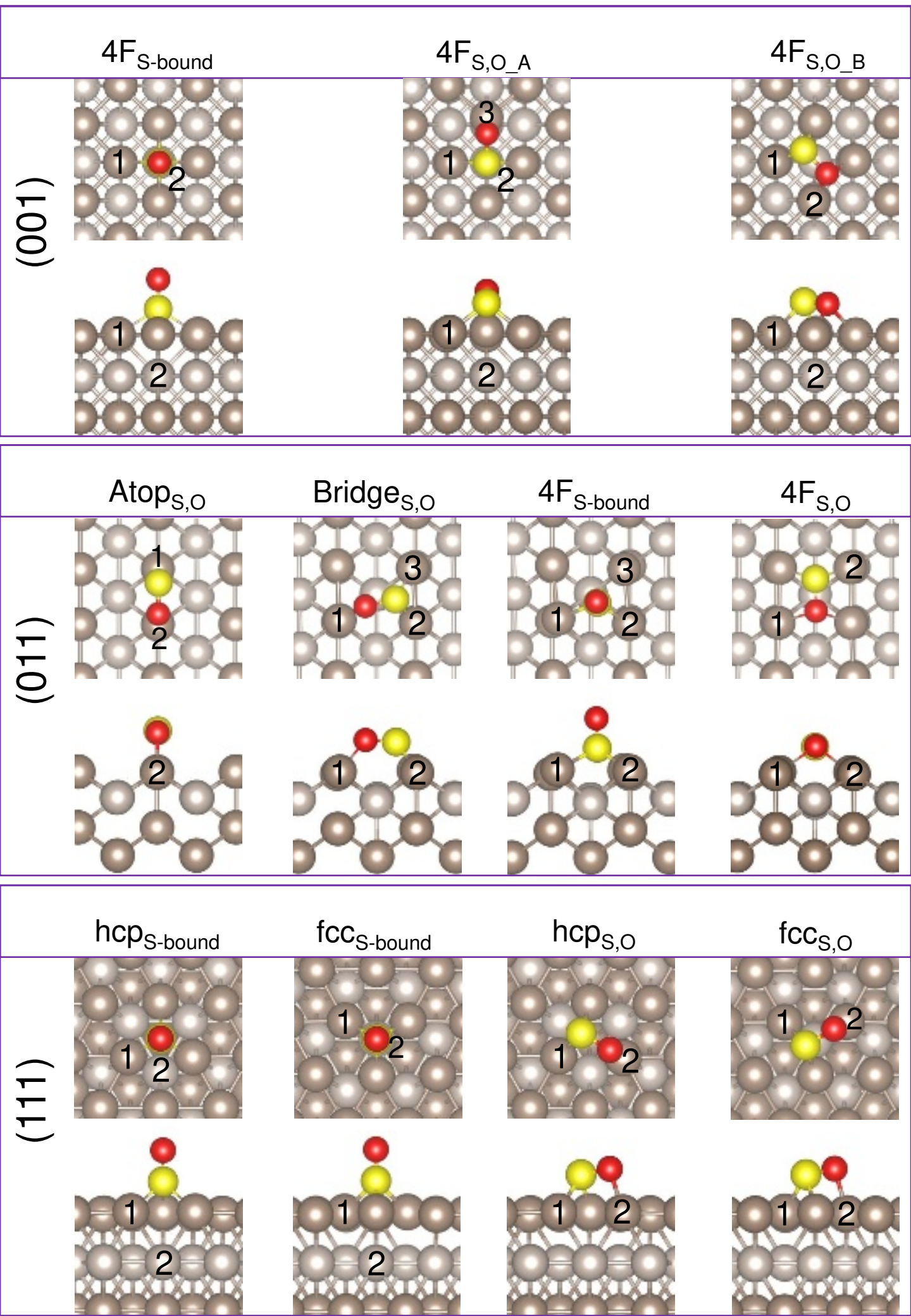


Pt (011)

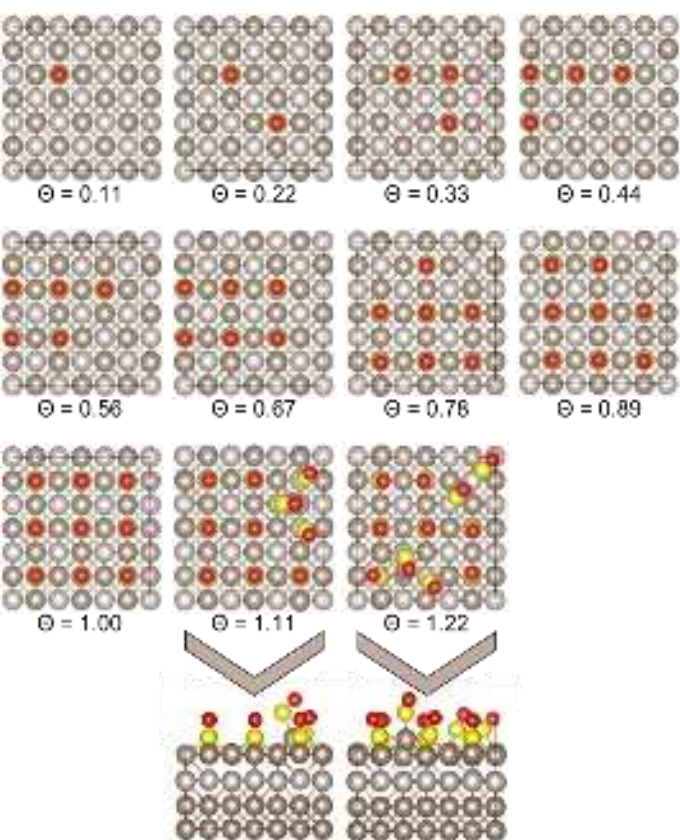




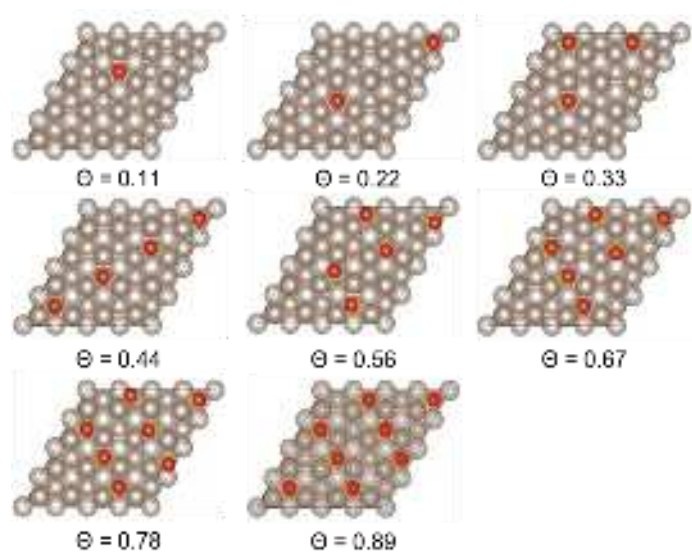




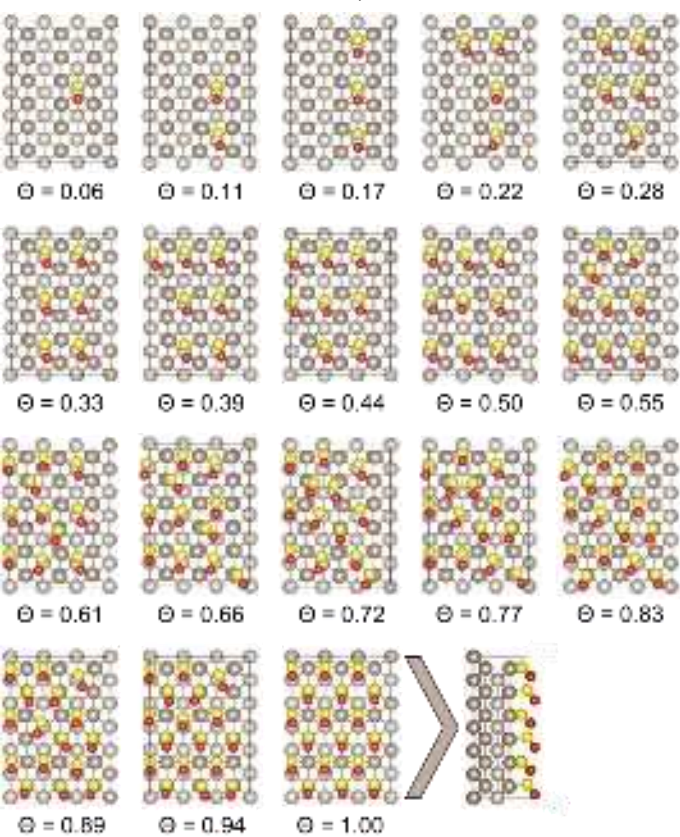
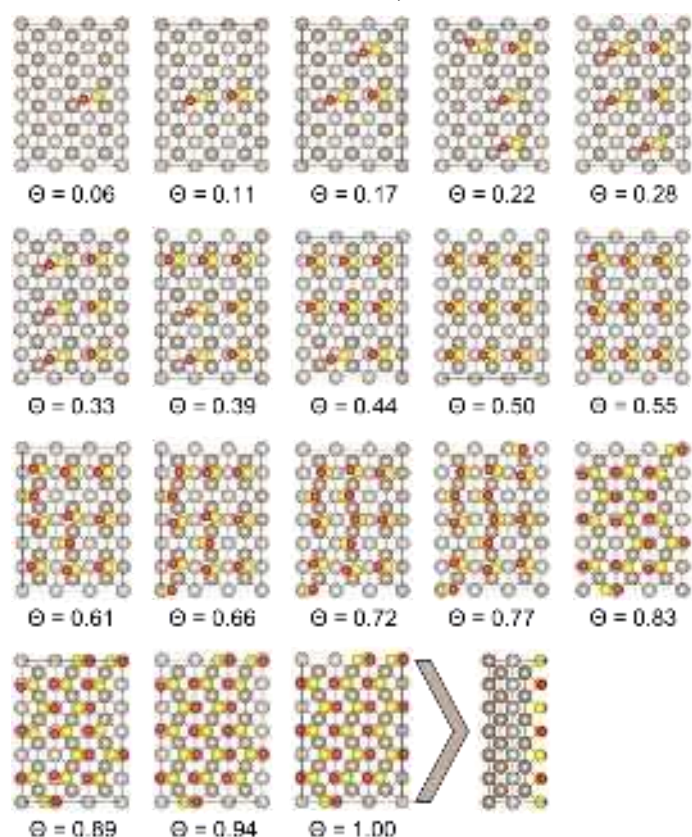
Pt (001)

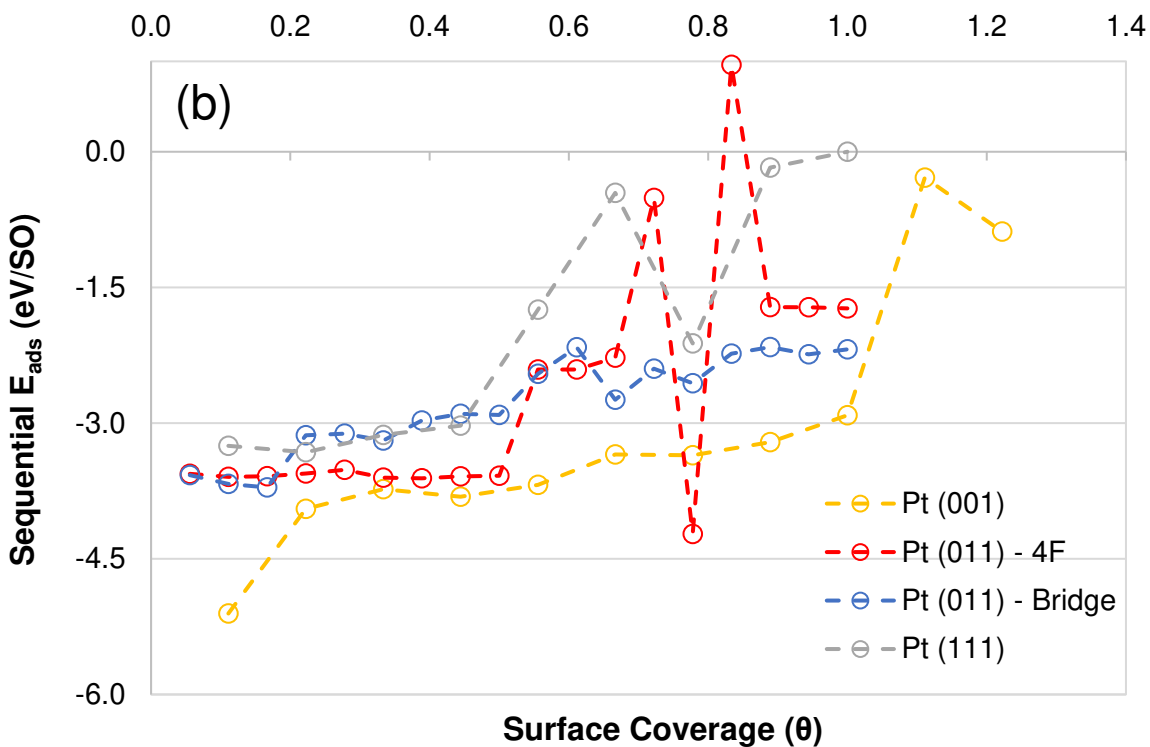
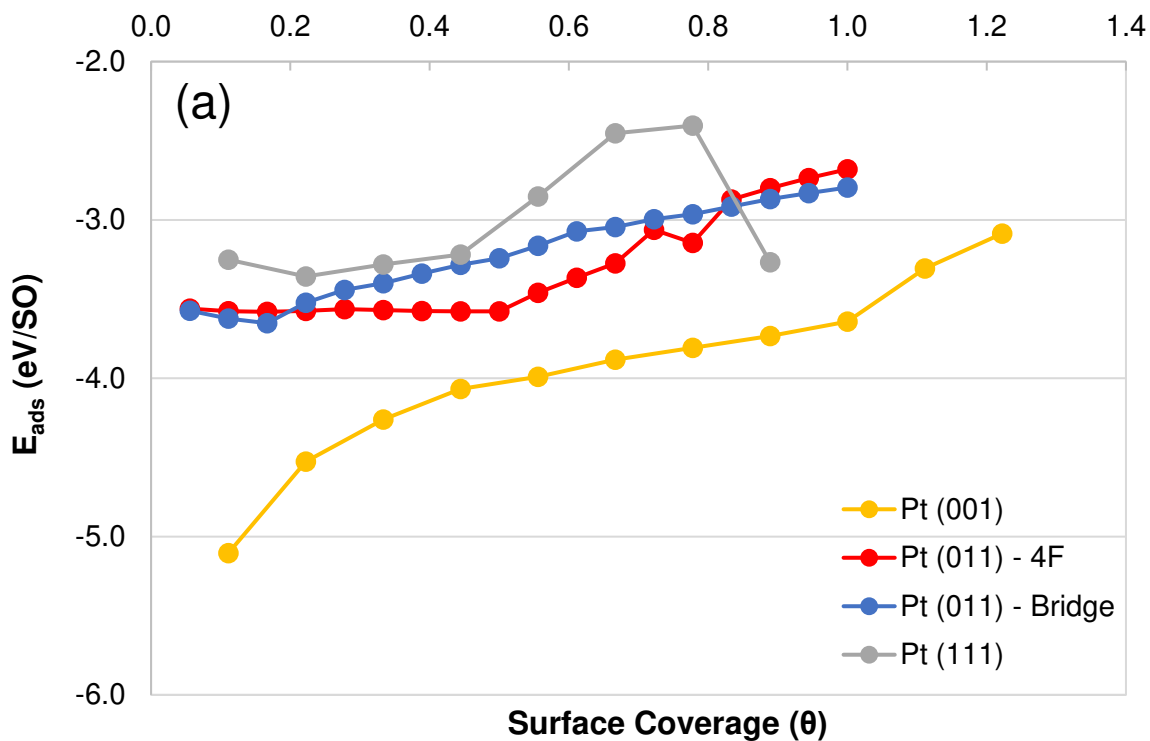


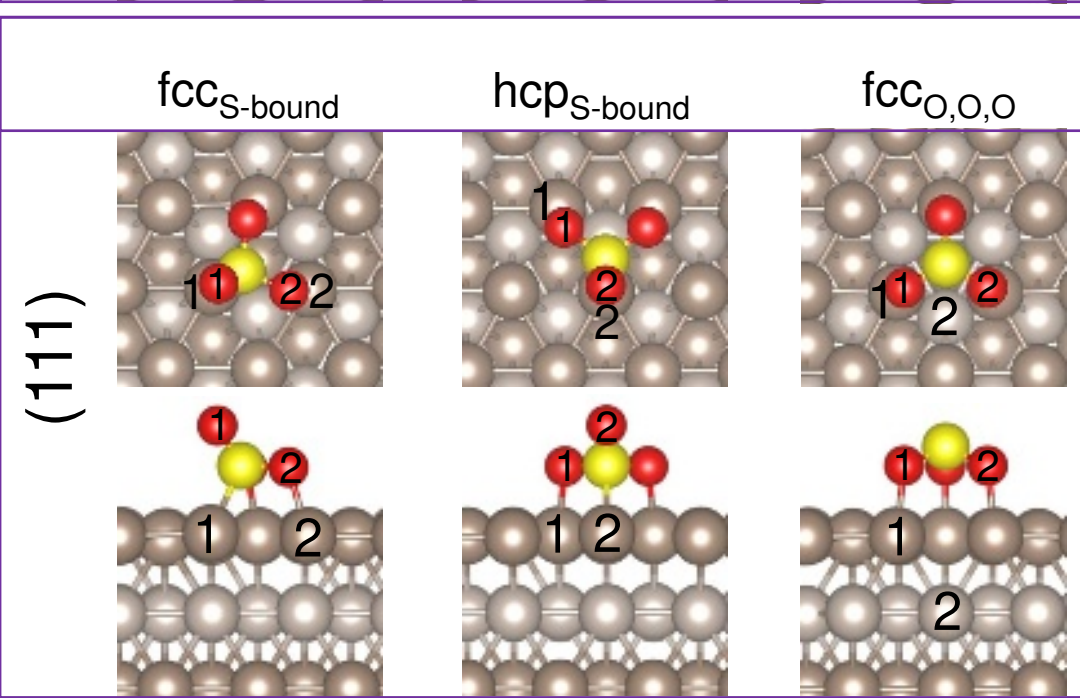
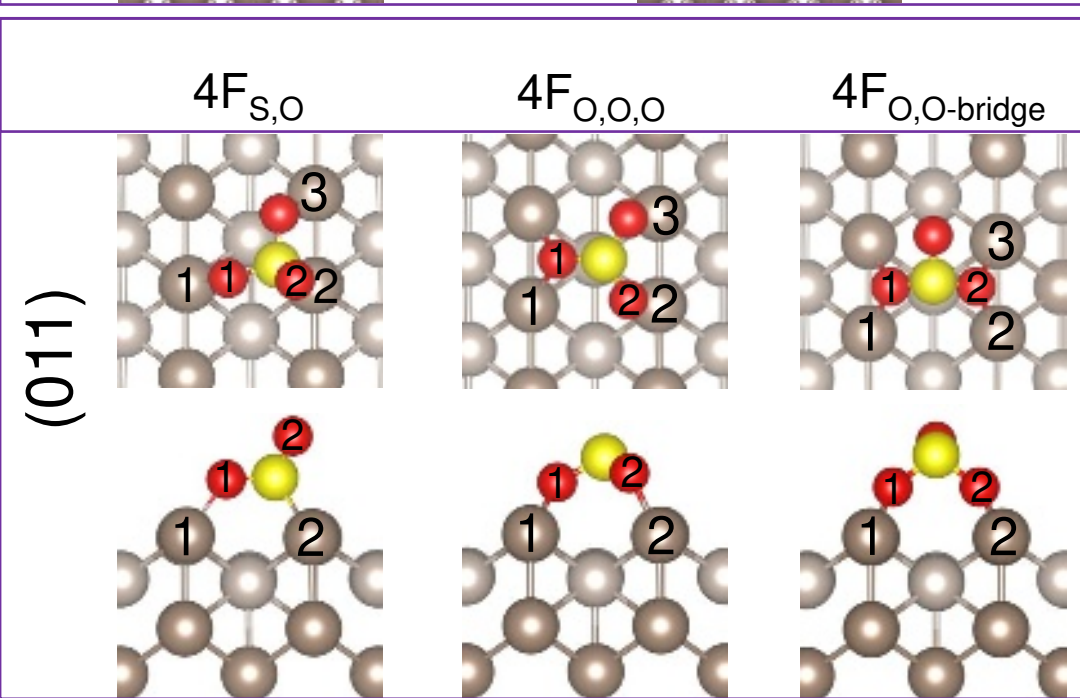
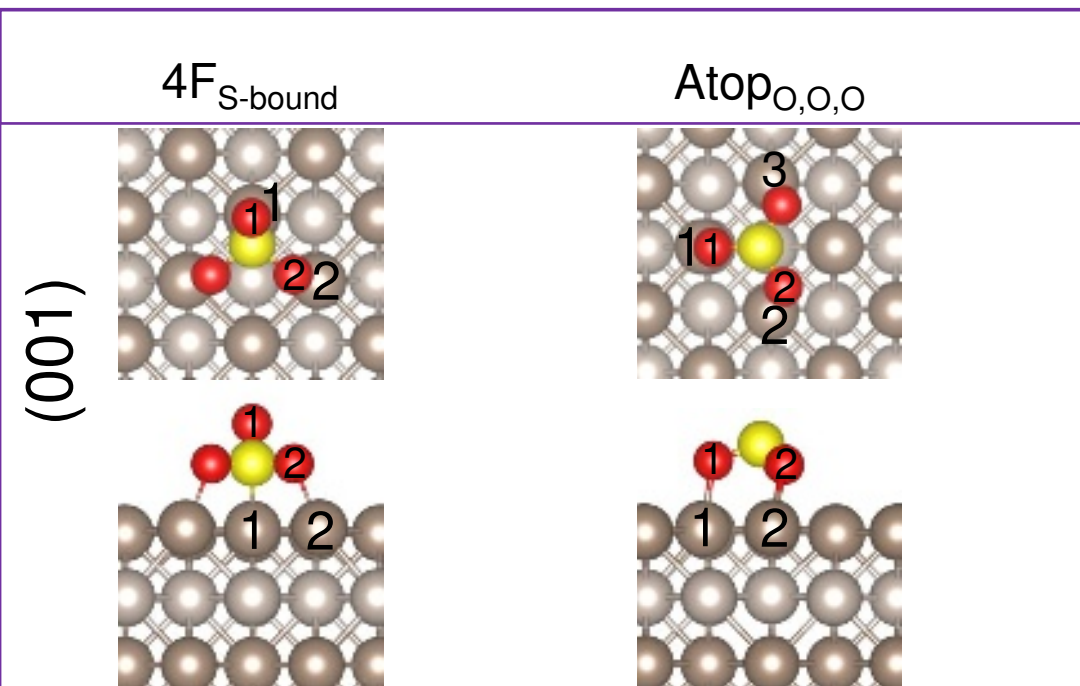
Pt (111)



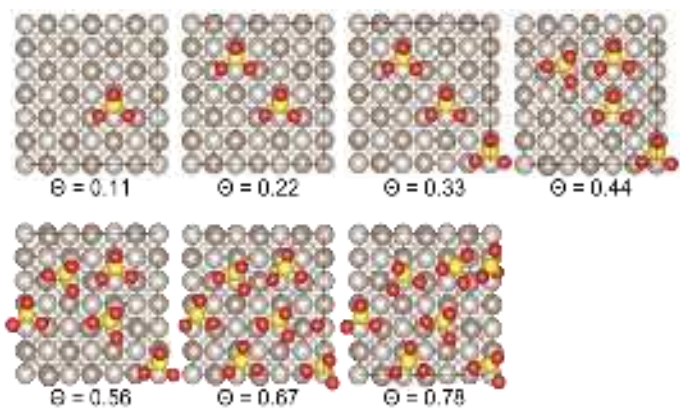
Pt (011)

 $4F_{S,O}$ Bridge<sub>S,O</sub>

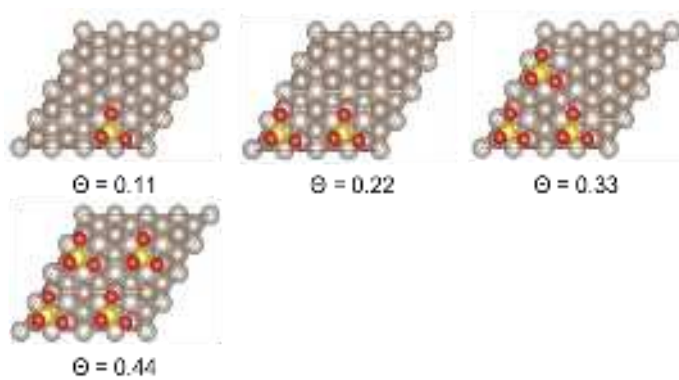




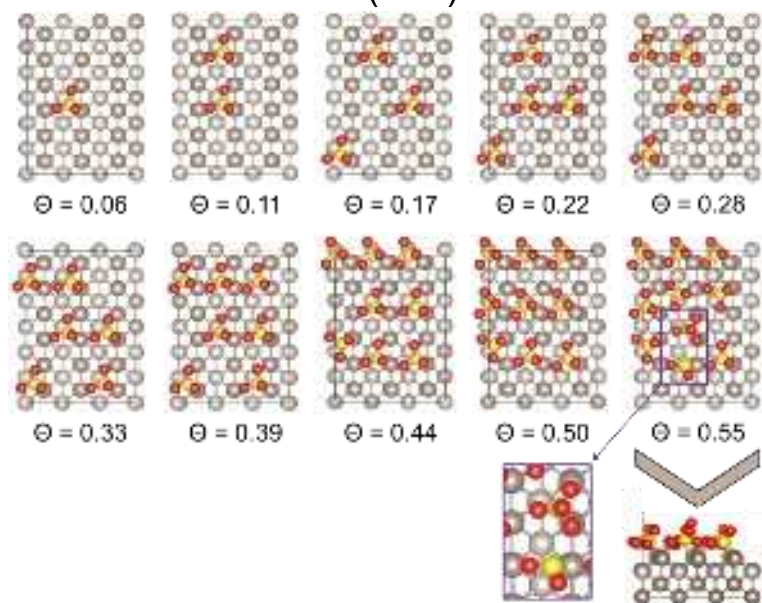
Pt (001)

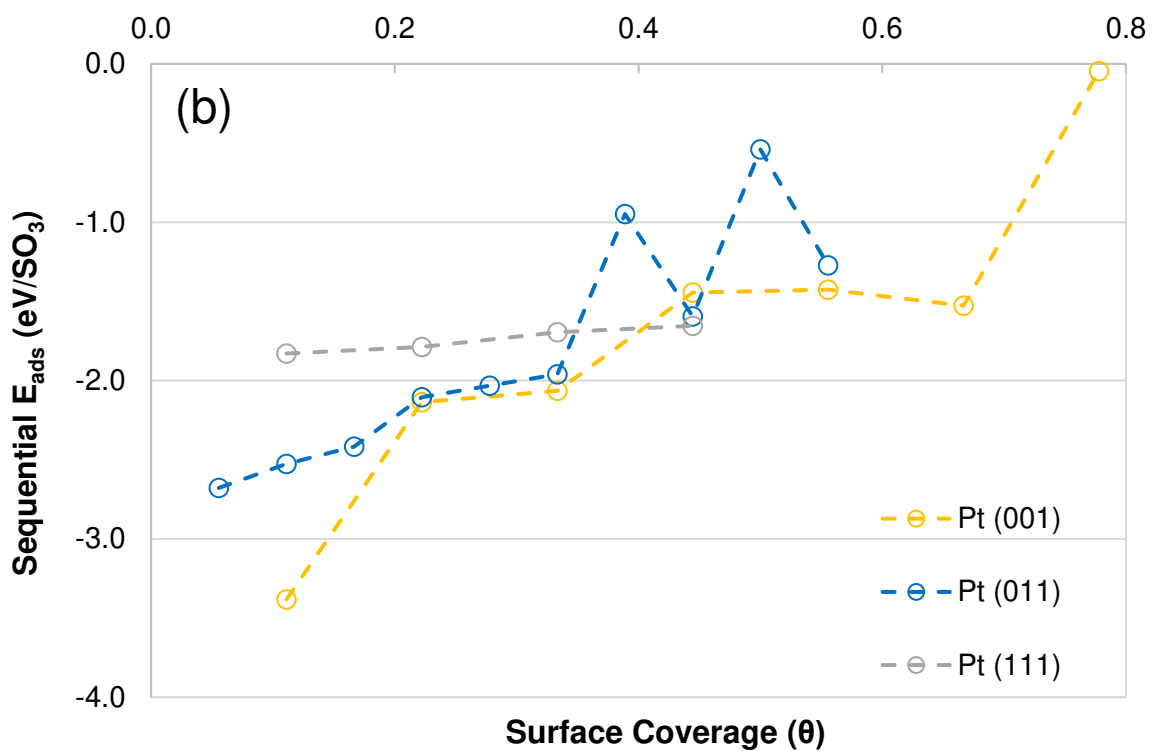
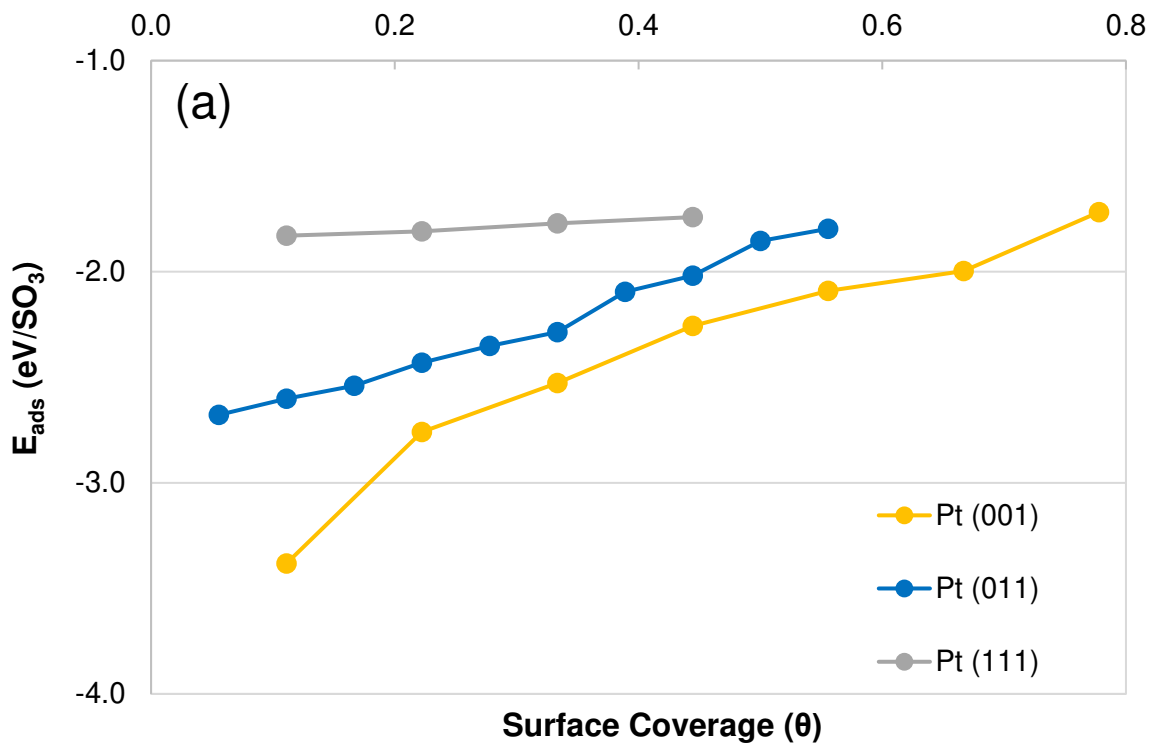


Pt (111)

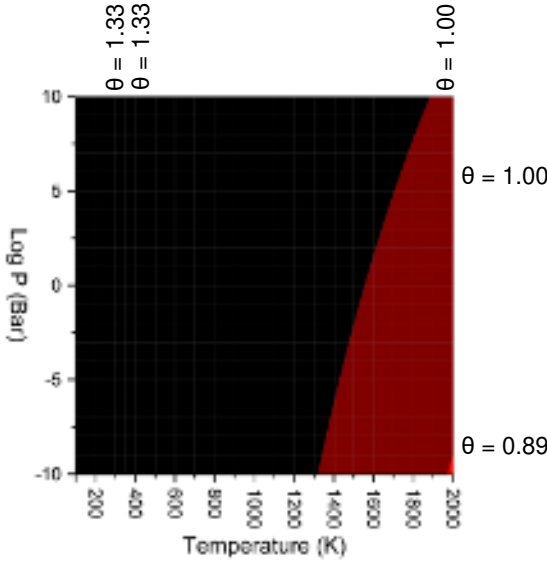


Pt (011)

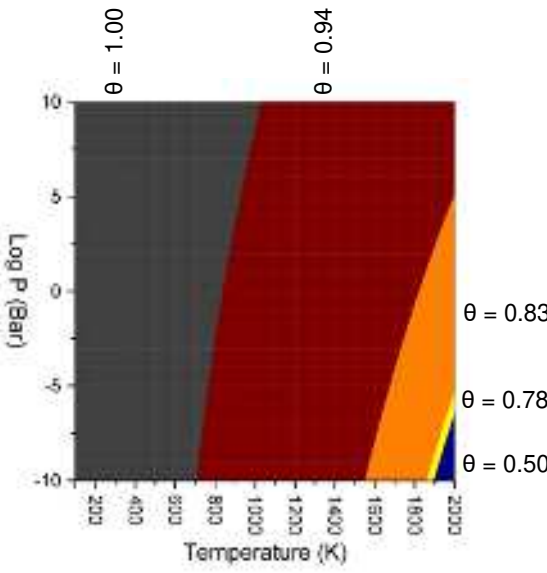




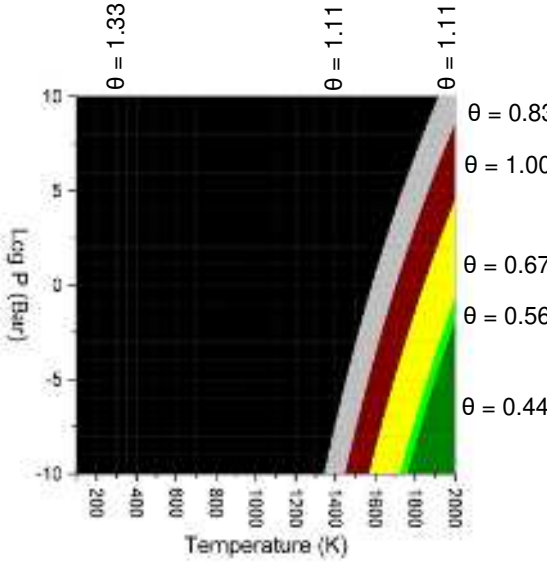
(001)



(011)

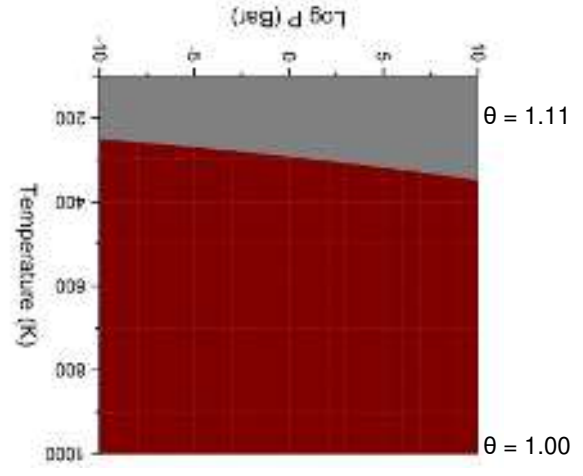


(111)

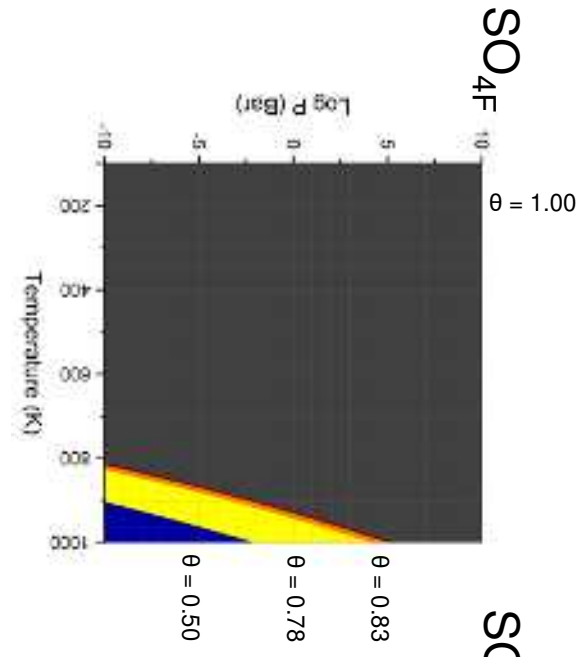




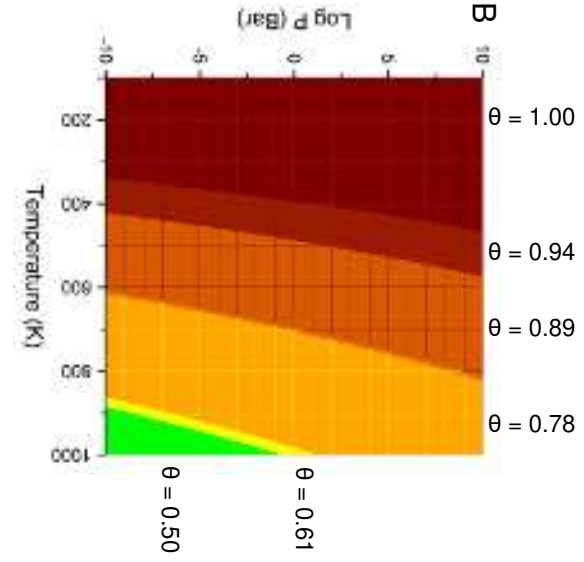
(001)



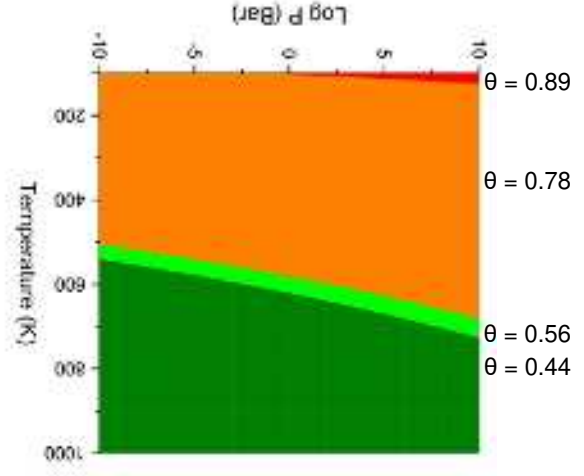
(011)



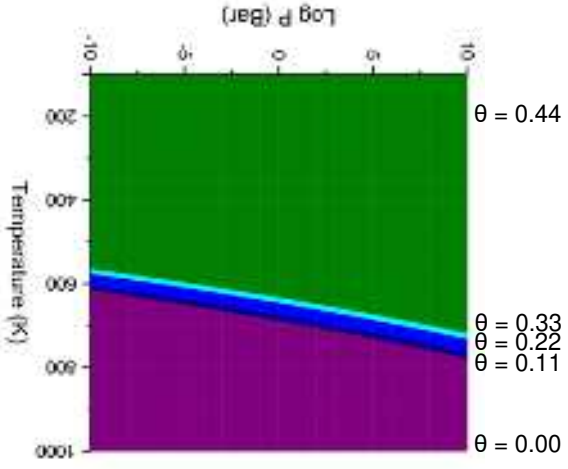
$\text{SO}_\text{B}$



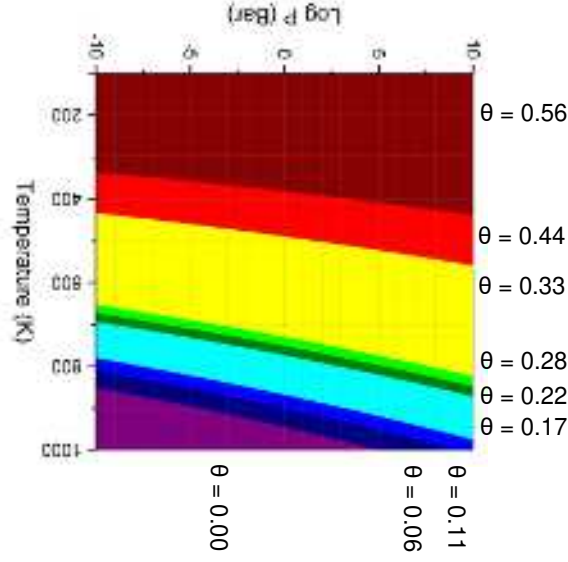
(111)



(111)



(011)



(001)

